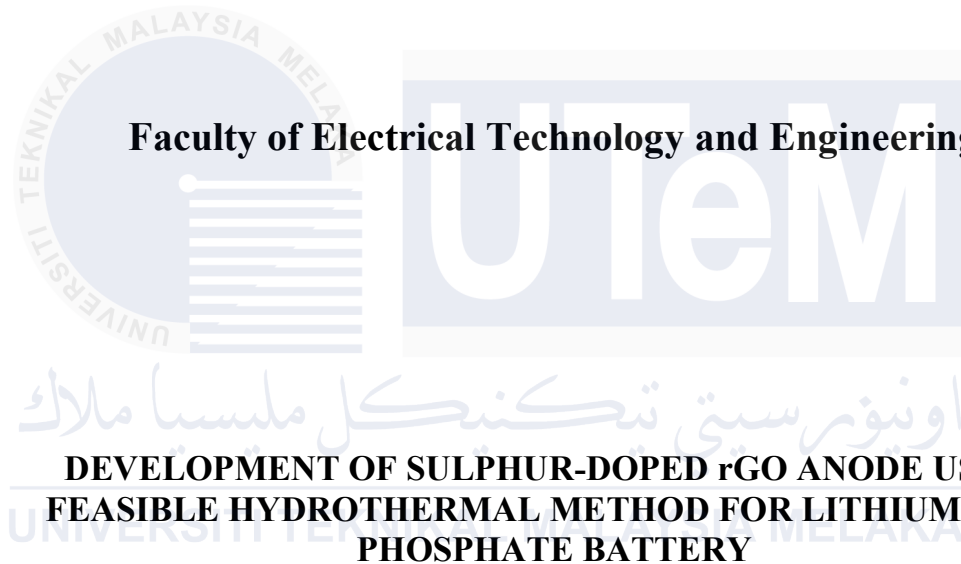




**Faculty of Electrical Technology and Engineering**



**DEVELOPMENT OF SULPHUR-DOPED rGO ANODE USING  
FEASIBLE HYDROTHERMAL METHOD FOR LITHIUM IRON  
PHOSPHATE BATTERY**

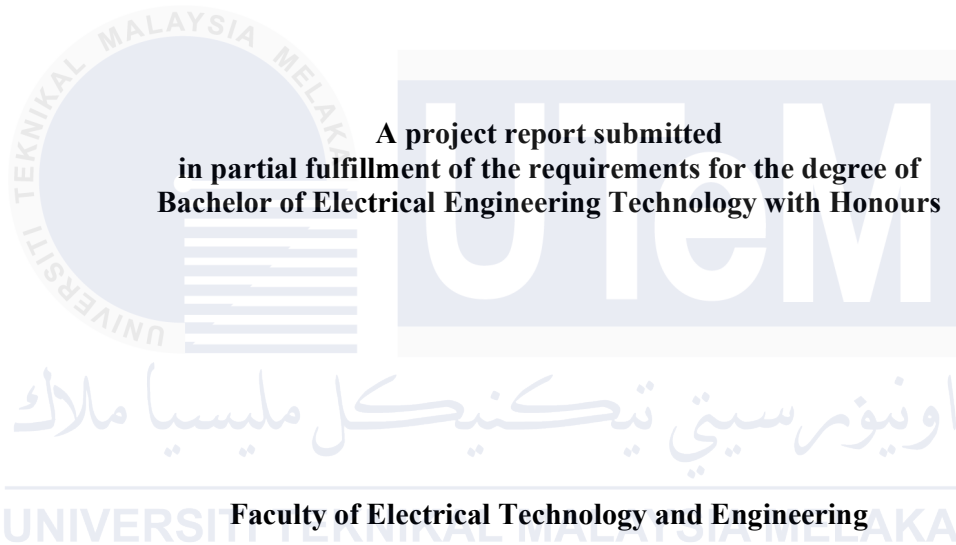
**SITI NUR AIN SALWANIE BINTI JAMALUDDIN**

**Bachelor of Electrical Engineering Technology with Honours**

**2025**

**DEVELOPMENT OF SULPHUR-DOPED rGO ANODE USING FEASIBLE  
HYDROTHERMAL METHOD FOR LITHIUM IRON PHOSPHATE BATTERY**

**SITI NUR AIN SALWANIE BINTI JAMALUDDIN**



**UNIVERSITI TEKNIKAL MALAYSIA MELAKA**

**2025**

## DECLARATION

I declare that this project report entitled “Development of Sulphur-Doped rGO Anode using Feasible Hydrothermal Method for Lithium Iron Phosphate Battery” is the result of my own research except as cited in the references. The project report has not been accepted for any degree and is not concurrently submitted in candidature of any other degree.



Signature :

Student Name : SITI NUR AIN SALWANIE BINTI JAMALUDDIN

Date : 3 JANUARY 2025

UNIVERSITI TEKNIKAL MALAYSIA MELAKA

## APPROVAL

I hereby declare that I have checked this project report and in my opinion, this project report is adequate in terms of scope and quality for the award of the degree of Bachelor of Electrical Engineering Technology with Honours.



Signature : \_\_\_\_\_

Supervisor Name : DR. NUR EZYANIE BINTI SAFIE

Date : 3/1/2024

UNIVERSITI TEKNIKAL MALAYSIA MELAKA

## DEDICATION

*To my beloved parents, who have been my strength throughout my academic journey. Your unconditional love, countless sacrifices, and endless encouragement have made it possible for me to reach this milestone. The values you instilled me have shaped who I am today.*

*To my mentor and thesis supervisor, Dr. Nur Ezynie Binti Safie, whose expertise constructive criticism, and unwavering support have been instrumental in bringing this research to success. Your passion for knowledge and commitment to academic excellence continue to inspire me.*

*To my friends and colleagues, who made this journey less lonely through countless study sessions, shared anxieties, and moment of success. Your companionship made the long hours of research and writing bearable.*

*This thesis stands as a testament to the collective support of all these wonderful people in my life.*

اونيورسيتي تيكنيكل مليسيا ملاك

UNIVERSITI TEKNIKAL MALAYSIA MELAKA

## ABSTRACT

The development of sulfur-doped reduced graphene oxide (S-rGO) using a feasible hydrothermal method for lithium iron phosphate battery also known as LFP battery is the main aim in this project. This research aims to develop a high-performance anode for LFP batteries via a facile hydrothermal process. Sulfur doping of reduced graphene oxide is one of the promising strategy to improve the lithium storage capacity, rate performance of the graphene anodes and to enhance the electrical conductivity of the battery. Sulfur-doped reduced graphene oxide leverages graphene's high conductivity and surface area, while sulfur doping creates defects and active sites to assist more lithium ions, increases interlayer spacing for improved ion diffusion, and facilitates faster kinetics reaction at the electrode-electrolyte interface. By using conductive additives and binders, the sulfur-doped reduced graphene oxide (S-rGO) will be composited to fabricate the anode electrode for incorporation into LFP coin cells under a glove box environment. Furthermore, to evaluate the electrochemical performance of the sulfur-doped reduced graphene oxide (S-rGO) anode in LFP coin cells, cyclic voltammetry and galvanostatic charge-discharge testing will be conducted thoroughly to estimate its potential as a high-capacity, cost-effective and durable anode material for next generation of the LFP batteries. Additionally, chassis car application will be used to observe the performance and stability of the coin cell batteries by analyzing voltage, current, and power delivery over time using real-time data.

## ***ABSTRAK***

Pembangunan graphene oksida terdop sulfur (S-rGO) menggunakan kaedah hidroterma yang boleh dilaksanakan untuk bateri litium fosfat iron juga dikenali sebagai bateri LFP adalah matlamat utama dalam projek ini. Penyelidikan ini bertujuan untuk membangunkan anod berprestasi tinggi untuk bateri LFP melalui proses hidroterma yang mudah. Pengdopan sulfur bagi graphene oksida yang dikurangkan adalah salah satu strategi yang menjanjikan untuk meningkatkan kapasiti penyimpanan litium, menilai prestasi anod graphene dan untuk meningkatkan kekonduksian elektrik bateri. Graphene oksida terdop sulfur memanfaatkan kekonduksian tinggi dan luas permukaan graphene, manakala doping sulfur mencipta kecacatan dan tapak aktif untuk membantu lebih banyak ion litium, meningkatkan jarak antara lapisan untuk penyebaran ion yang lebih baik dan memudahkan tindak balas kinetik yang lebih pantas pada antara muka elektrod-elektrolit. Dengan menggunakan bahan tambahan dan pengikat konduktif, graphene oksida terdop sulfur (S-rGO) akan digubah untuk menghasilkan elektrod anod untuk dimasukkan ke dalam sel syiling LFP di bawah persekitaran kotak sarung tangan. Tambahan pula, untuk menilai prestasi elektrokimia anod graphene oxide (S-rGO) terkurang doped sulfur dalam sel syiling LFP, voltammetri kitaran dan ujian nyahcas galvanostatik akan dijalankan secara menyeluruh untuk menganggarkan potensinya sebagai kapasiti tinggi, kos- bahan anod yang berkesan dan tahan lama untuk generasi seterusnya bateri LFP. Selain itu, aplikasi kereta casis akan digunakan untuk memerhati prestasi dan kestabilan bateri sel syiling dengan menganalisis voltan, arus dan penghantaran kuasa dari semasa ke semasa menggunakan data masa nyata.

## ACKNOWLEDGEMENTS

First and foremost, I would like to express my gratitude to my supervisor, Dr. Nur Ezyanie Binti Safie for the precious guidance, words of wisdom and patient throughout this project.

I am also indebted to Universiti Teknikal Malaysia Melaka (UTeM) and Dr. Nur Ezyanie Binti Safie for the financial support through funding all the components needed which enables me to accomplish the project. Not forgetting my fellow colleague, for the willingness of sharing his thoughts and ideas regarding the project.

My highest appreciation goes to my parents, and family members for their love and prayer during the period of my study. An honourable mention also goes to my fellow friends for all the motivation and understanding.

Finally, I would like to thank all the staffs at the Universiti Teknikal Malaysia Melaka (UTeM), fellow colleagues and classmates, the faculty members, as well as other individuals who are not listed here for being co-operative and helpful.

## TABLE OF CONTENTS

	PAGE
<b>DECLARATION</b>	
<b>APPROVAL</b>	
<b>DEDICATIONS</b>	
<b>ABSTRACT</b>	i
<b>ABSTRAK</b>	ii
<b>ACKNOWLEDGEMENTS</b>	iii
<b>TABLE OF CONTENTS</b>	4
<b>LIST OF TABLES</b>	6
<b>LIST OF FIGURES</b>	7
<b>LIST OF SYMBOLS</b>	8
<b>LIST OF ABBREVIATIONS</b>	9
<b>CHAPTER 1 INTRODUCTION</b>	<b>11</b>
1.1 Background	11
1.2 Sustainable Development Goals (SDGs)	14
1.3 Problem Statement	15
1.4 Project Objective	17
1.5 Scope of Project	17
1.6 Significant Research	18
1.7 Thesis Organization	19
<b>CHAPTER 2 LITERATURE REVIEW</b>	<b>20</b>
2.1 Introduction	20
2.2 Lithium-Ion Battery (LIB)	21
2.2.1 Type Of Lithium-Ion Battery (LIB)	22
2.2.2 Lithium Iron Phosphate (LFP) Battery	25
2.3 Mechanism of LFP	27
2.3.1 Battery Structure	29
2.3.2 Comprehensive Review of Anode Materials	31
2.4 Graphene as Anode Materials	34
2.4.1 Type of Functionalized Graphene	35
2.4.1.1 Graphene Oxide (GO)	36
2.4.1.2 Reduced Graphene Oxide ( rGO )	37
2.4.1.3 Sulfur-doped Reduced Graphene Oxide ( S-rGO )	38
2.5 Electrochemical Performance	39
2.5.1 Cyclic Voltammetry (CV)	40

2.5.2	Galvanostatic Charge-Discharge (GCD)	44
2.6	Summary	49
<b>CHAPTER 3 METHODOLOGY</b>		<b>50</b>
3.1	Introduction	50
3.1.1	Research Design	50
3.2	Preparation of Functionalized Graphene Anode	54
3.2.1	Synthesis of Graphene	54
3.2.2	Synthesis of S-doped Graphene	55
3.2.3	Preparation of S-doped Graphene Anode Film	55
3.3	Fabrication of Full-cell Coin Cell Battery	57
3.4	Electrochemical Performance Evaluation	59
3.4.1	Cyclic Voltammetry (CV)	60
3.4.2	Galvanostatic Charge Discharge (GCD)	61
3.5	Experimental Setup to Validate Battery Performance	62
3.5.1	List of Components	64
3.6	Summary	65
<b>CHAPTER 4 RESULTS AND DISCUSSIONS</b>		<b>66</b>
4.1	Introduction	66
4.2	Electrochemical Performance	67
4.3	Battery Performance Validation	70
4.4	Summary	77
<b>CHAPTER 5 CONCLUSION</b>		<b>79</b>
5.1	Conclusion	79
5.2	Potential Commercialization	80
<b>REFERENCES</b>		<b>82</b>

## LIST OF TABLES

TABLE	TITLE	PAGE
Table 3.1	Components used for the experiment.	64
Table 4.1	Voltages and currents over time data collected through chassis car application.	71



## LIST OF FIGURES

FIGURE	TITLE	PAGE
Figure 1.1:	Shapes of LIBs	13
Figure 1.2:	Coin Cell Assembly	14
Figure 2.1:	Applications of Lithium-Ion Battery	22
Figure 2.2:	LFP Battery	27
Figure 2.3:	LFP Battery Structure	30
Figure 2.4:	(a) The CV curves of 65% Si nanoparticles/35% graphene composite, $V = 0.1 \text{ mV/s}$ . 1st to 5th cycle [19]. (b) SCF@rGO/S at various scan rates [20]. (c) CV tests of the S80FLG20 [21]. (d) CVs at the scan rate of $0.1 \text{ mV s}^{-1}$ up to three cycles and estimation of the area under the CV curves [22]. (e) CV curves of Pure GA and GA/[1]G-2-1 at different scan rates [23].	43
Figure 2.5:	(a) At $100 \text{ mA/g}$ , GCD voltage profiles at $100 \text{ mA/g}$ [25]. (b) GCD for $\text{GeO}_2/\text{Ge75/r-GO}$ [12]. (c) The GCD profile of the composite $\text{CuS/GO}$ electrode at varied current densities, (inset image shows the LIB device demonstration) [26]. (d) ) GCD profiles of NPHG cathode at $0.1, 0.2, 0.5,$ and $1 \text{ A/g}$ [24]. (e) The GCD profiles for the first cycle at a current rate of $0.1\text{C}$ [27].	48
Figure 3.1:	Flowchart of the project	53
Figure 3.2:	The construction of coin cell 2032 components [28]	58
Figure 3.3:	Chassis car assembled for battery performance.	63
Figure 3.4:	Arduino connection diagram for battery performance.	63
Figure 4.1:	Electrochemical performance: (a) cyclic voltammetry (CV) of cycle 1 to 3 at scan rate of $0.2 \text{ mV/s}$ from $0.01$ to $3.00 \text{ V}$ , (b) discharge/charge curves of the first ten cycles at current density $100 \text{ mA/g}$ , (c) cyclic stability at current density $100 \text{ mA/g}$ , and (d) energy density measurement at current density $100 \text{ mA/g}$ .	67
Figure 4.2:	Voltage over time trends for three samples A, B, and C.	73
Figure 4.3:	Current profiles for three samples A,B, and C.	74
Figure 4.4:	Power output comparison for three samples A, B, and C.	76

## LIST OF SYMBOLS

%	-	Percentage
°C	-	Degree celcius
$\Delta E$	-	Voltage difference
°	-	Degree angle
$\theta$	-	Thetha
Å	-	Angstrom wavelength
$e^-$	-	Negative electron
$Li^+$	-	Lithium ions



## LIST OF ABBREVIATIONS

<i>LIB</i>	-	Lithium-ion battery
<i>LFP</i>	-	Lithium iron phosphate battery
<i>LiFePO<sub>4</sub></i>	-	Lithium iron phosphate
<i>LMO</i>	-	Lithium manganese oxide
<i>NMC</i>	-	Lithium nickel manganese cobalt oxide
<i>Li<sub>4</sub>Ti<sub>5</sub>O<sub>12</sub></i>	-	Lithium titanate
<i>EC</i>	-	Ethylene carbonate
<i>DMC</i>	-	Dimethyl carbonate
<i>SDG(s)</i>	-	Sustainable Development Goal(s)
<i>SDG 7</i>	-	Sustainable Development Goal 7
<i>S-rGO</i>	-	Sulfur-doped reduced graphene oxide
<i>CB</i>	-	Carbon black
<i>GO</i>	-	Graphene oxide
<i>rGO</i>	-	Reduced graphene oxide
<i>CV</i>	-	Cyclic voltammetry
<i>GCD</i>	-	Galvanostatic charge-discharge (GCD)
<i>Li<sup>+</sup></i>	-	Lithium ions
<i>FePO<sub>4</sub></i>	-	Iron phosphate
<i>Li</i>	-	Lithium
<i>LiPF<sub>6</sub></i>	-	Lithium hexafluorophosphate
<i>LiBF<sub>4</sub></i>	-	Lithium tetrafluoroborate
<i>EV</i>	-	Electric vehicle
<i>SEI</i>	-	Solid-electrolyte interphase
<i>mAh/g</i>	-	Milliamperes-hours of charge per gram
<i>SnO<sub>2</sub></i>	-	Tin dioxide
<i>TiO<sub>2</sub></i>	-	Titanium dioxide
<i>MnO<sub>2</sub></i>	-	Manganese dioxide
<i>Sn</i>	-	Tin
<i>Si</i>	-	Silicon
<i>V</i>	-	Voltage
<i>C</i>	-	Coulomb
<i>vs</i>	-	Versus
<i>Scm<sup>-1</sup></i>	-	Siemens per centimetre
<i>cm<sup>2</sup> s<sup>-1</sup></i>	-	Square centimetres per second
<i>TMOs</i>	-	Transition metal oxides
<i>CVD</i>	-	Chemical vapor deposition
<i>2D</i>	-	Two-dimensional
<i>mV/s</i>	-	Millivolt per second
<i>LiPSs</i>	-	Lithium polysulfides
<i>SCF@rGO/S</i>	-	Self-supporting carbon framework modified by reduced graphene oxide with sulfur
<i>SCF/S</i>	-	Self-supporting carbon framework with sulfur
<i>PPC/S</i>	-	Powdery porous carbon with sulfur
<i>wt%</i>	-	Weight percent
<i>G/Al</i>	-	Graphene/aluminium
<i>V<sub>2</sub>O<sub>3</sub>/G/Al</i>	-	Vanadium trioxide/graphene/aluminium

<i>Sn-V<sub>2</sub>O<sub>3</sub>/G/Al</i>	-	Tin doped Vanadium trioxide/graphene/aluminium
<i>V<sub>2</sub>O<sub>3</sub></i>	-	Vanadium trioxide
<i>GA</i>	-	Glutaraldehyde
<i>GA-G-2-1</i>	-	Glutaraldehyde with graphene for mass raatio 2:1
<i>mA/g</i>	-	miliAmpere per gram
<i>MoS<sub>2</sub></i>	-	Molybdenum disulfide
<i>GeO<sub>2</sub>/Ge/r-GO</i>	-	Germanium oxide with gremanium reduced graphene oxide
<i>mA</i>	-	miliAmpere
<i>Ge25</i>	-	Germanium 25 anion
<i>Ge50</i>	-	Germanium 50 anion
<i>Ge75</i>	-	Germanium 75 anion
<i>CuS/GO</i>	-	Copper(II) sulfide graphene oxide
<i>CuS</i>	-	Copper(II) sulfide
<i>NPHG</i>	-	Nitrogen and phosphorus co-doped hierarchical porous graphene
<i>IR</i>	-	Insulation resistance
<i>HG</i>	-	hierarchical graphene
<i>F g<sup>-1</sup></i>	-	Farad per gram
<i>A g<sup>-1</sup></i>	-	Ampere per gram
<i>NCS@S</i>	-	Nanocrystal sulfide
<i>NCS@rGO@S</i>	-	Nanocrystal reduced graphene oxide sulfide
<i>mL</i>	-	miliLitre
<i>pH</i>	-	potential Hydrogen
<i>M</i>	-	Molar
<i>g/mL</i>	-	Gram per miliLitre
<i>AB</i>	-	Acetylene black
<i>PVDF</i>	-	Polyvinylidene fluoride
<i>NMP</i>	-	N-methyl pyrrolidone
<i>g</i>	-	Gram
<i>mm</i>	-	milimetre
<i>kg/cm<sup>2</sup></i>	-	Kilogram per square centimetre
<i>G-band</i>	-	Graphitic carbon
<i>D-band</i>	-	Disordered carbon
<i>nm</i>	-	Nanometre
<i>mW</i>	-	miliWatt
<i>I<sub>D</sub>/I<sub>G</sub></i>	-	The ratio of the D-band and G-band
<i>I<sub>2D</sub>/I<sub>G</sub></i>	-	The ratio of the intensities of the 2D-band and G-band
<i>kV</i>	-	kiloVolt

# CHAPTER 1

## INTRODUCTION

### 1.1 Background

Nowadays, renewable energy, such as solar and wind power, is essential in reducing greenhouse gas emissions and climate change. These sources have gained the attention of society in recent years because they are not only abundant but also clean, making them essential components of a sustainable energy future. Their intermittent nature poses a few challenges to our grid stability and energy storage system. Energy storage plays a crucial role in covering up the intermittent of renewable energy sources. These technologies store the excess energy generated during peak production times and release the energy when there is high demand or when needed. Various energy storage solutions are being employed all over the world, such as batteries like lithium-ion batteries (LIBs), to implement an efficient energy storage system.

A lot of improvements can be made to increase the performance of the lithium iron phosphate (LFP) batteries, also known as LFP batteries, because they are often limited by the anode materials. LFP batteries are a specific type of rechargeable lithium-ion battery (LIB) renowned for their outstanding safety and extended lifespan. Unlike traditional LIBs, LFP batteries employ lithium iron phosphate ( $\text{LiFePO}_4$ ) as the cathode material, providing inherent stability and resistance against thermal runaway. This quality diminishes the risk of fire or explosion, even in challenging environments. Such a safety feature renders LFP batteries highly sought-after for critical applications where dependability is paramount, such as in electric vehicles and energy storage systems. Furthermore, LFP batteries boast an extended cycle life compared to alternative lithium-ion formulations, enduring many charge-

discharge cycles without significant deterioration. While they may own marginally lower energy density than certain lithium-ion counterparts, LFP batteries prove superior performance in high-temperature settings and keep a reduced self-discharge rate, ensuring prolonged charge retention during periods of inactivity. Consequently, LFP batteries are extensively used across diverse industries, including electric transportation, renewable energy storage, and specific portable electronics, due to their prized attributes of safety, longevity, and resistance to thermal challenges.

Graphite is commonly used as an anode in these LIBs where the lithium iron phosphate works as the cathode. Graphite has interlayer spacing where the layered structure basically provides interlayer spaces where lithium ions can intercalate and deintercalated reversibly during charge and discharge cycles. Graphite also has good cycling stability, keeping its performance and structure. Additionally, graphite is inexpensive compared to some alternative anode materials. Ongoing research aims to further enhance the performance of graphite anodes by improving their specific capacity, rate capability, and cycling stability.

Graphene, characterized by its two-dimensional lattice of carbon atoms arranged in a honeycomb structure, shows an array of remarkable properties. Notably, it shows exceptional carrier mobility, allowing electric charge carriers to move remarkably easily. Its thermal conductivity is unparalleled, easing efficient heat transfer. Graphene's electronic structure features linear dispersion at the K-point, contributing to its unique electronic properties. Moreover, it owns a vast specific surface area, providing ample space for various interactions. Additionally, graphene displays immensely high intrinsic strength, making it incredibly resilient to mechanical stress.

There are a few shapes of lithium-ion batteries, such as cylindrical, prismatic, pouches and coin cells (Figure 1.1). The primary elements employed in LIBs include the anode, cathode, and electrolyte (Figure 1.2). The LFP batteries work on the principle of

lithium-ion moving between the anode and cathode electrodes during the charging and discharging process. Firstly, the cathode is the positive electrode that undergoes an oxidation process during the discharge process and the reduction process during the charging process in lithium-ion batteries. The common materials used as cathode are lithium manganese oxide (LMO), lithium nickel manganese cobalt oxide (NMC) and lithium iron phosphate (LFP). The anode is the negative electrode that stores and releases lithium ions during the charging and discharging processes, respectively. Typically, the anode material is carbon-based like graphite and others like lithium titanate ( $\text{Li}_4\text{Ti}_5\text{O}_{12}$ ), silicon and silicon-based materials. The electrolyte is an ionic conductive solution that allows lithium ions to flow between the anode and cathode. It typically consists of lithium salt dissolved in an organic solvent mixture, such as ethylene carbonate (EC) and dimethyl carbonate (DMC). The electrolyte must be chemically and electrochemically stable within the operating voltage range of the battery.

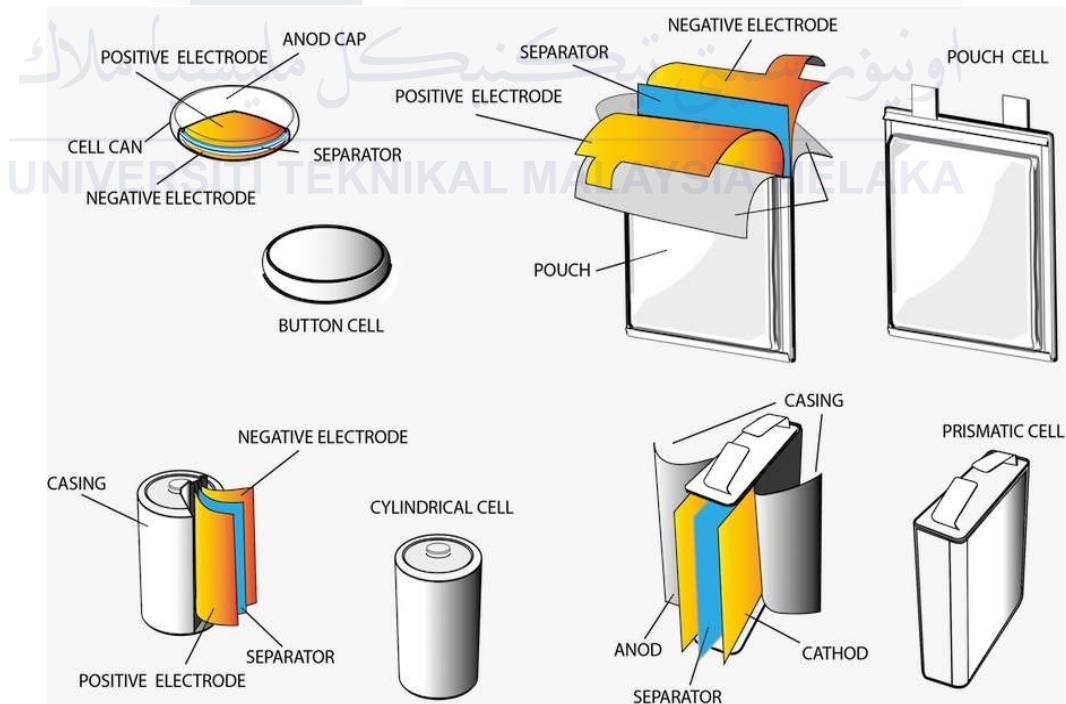


Figure 1.1: Shapes of LIBs

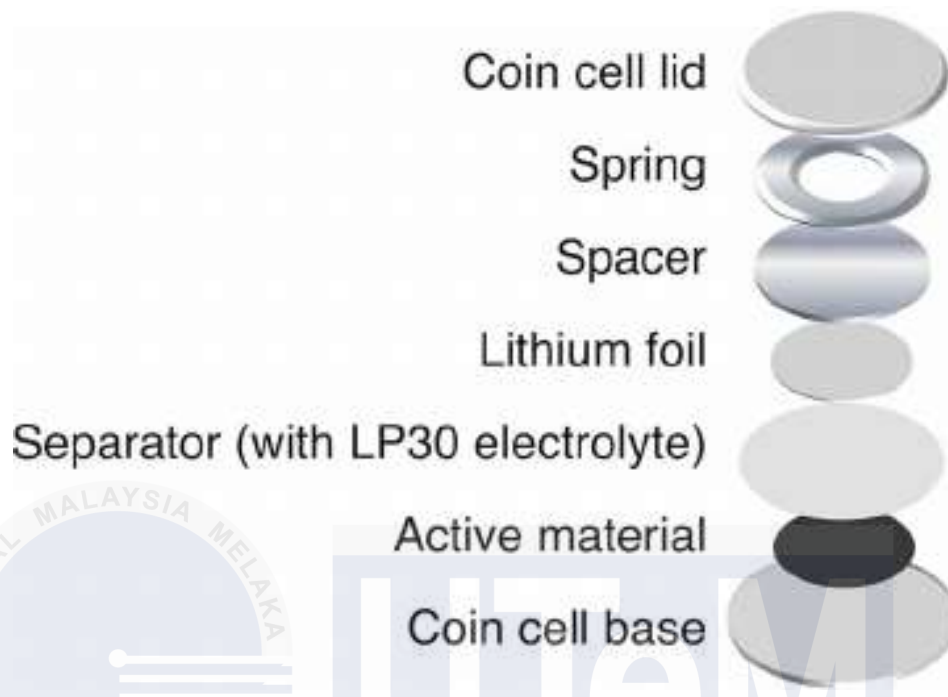


Figure 1.2: Coin Cell Assembly

To conclude, the choice of anode materials plays a crucial role in optimizing the LFP battery's performance. It will significantly affect their overall performance, safety, cost, and environmental impact. The anode materials will determine the battery's energy capacity, cycle life, rate capability, and voltage stability, affecting its efficiency and longevity. Certain materials can mitigate safety risks associated with dendrite formation, ensuring reliability. Anode costs basically influence battery manufacturing expenses while considerations such as material abundance and recyclability contribute to environmental sustainability.

## 1.2 Sustainable Development Goals (SDGs)

The creation of a sulfur-doped reduced graphene oxide (S-rGO) anode through a practical hydrothermal method for LFP batteries significantly contributes to achieving Sustainable Development Goal 7 (SDG 7): Affordable and Clean Energy. The intended research aims to improve the performance and sustainability of LIBs, which are vital for the

widespread use of renewable energy sources and the transition to electric transportation. By enhancing the energy density and lifespan of LFP batteries, this research facilitates the effective storage of intermittent renewable energy, thereby increasing the proportion of renewable energy in the global energy mix. This, in turn, aids in reducing greenhouse gas emissions and addressing climate change. Additionally, the use of a hydrothermal method for producing the sulfur-doped reduced graphene oxide (S-rGO) anode is an eco-friendly and cost-efficient approach, aligning with the principles of sustainable development. Overall, this research has the potential to expedite the shift to a low-carbon economy, ensuring universal access to affordable, dependable, and sustainable energy, which is the fundamental objective of SDG 7.

### **1.3 Problem Statement**

Lithium iron phosphate (LFP) batteries, also referred to as LFP batteries, significantly attract the interest of the world due to their inherent safety, long life cycle, environmental friendliness, and stability. Unfortunately, LFP batteries have poor electronic conductivity and low lithium-ion diffusion. LFP batteries have lower energy density compared to other LIBs. This battery only has a lower capacity to store energy per unit volume or weight resulting in larger and heavier battery packs for the same value of energy storage capacity. These restrictions affected the performance of the battery. Its performance is also limited due to the anode materials. Therefore, graphene is being used as the anode material to boost the battery's performance. Graphene is a type of novel and powerful planar conductive additive and has been considered one of the promising conductive additives for both positive and negative electrodes in LIBs to partly or even completely replace the existing carbon black (CB), due to its unique physical and chemical properties, high aspect ratio, chemical tolerance, excellent electrical conductivity and effective conducting network

at even a trace amount. Therefore, the electronic conductivity of the electrodes can be improved with a much smaller amount of graphene as a conductive additive [1]. Using graphene as the anode material also has a negative impact where the graphene structure itself will affect the lithium-ion diffusion by showing a steric hindrance effect. Additionally, the GO-based composite electrodes have poor electrical conductivity due to defects and residual oxygen-containing groups [2]. However, achieving its effectiveness depends on the development of cost-effective superficial techniques to synthesize high-quality, large-area graphene. Significant efforts are needed to devise techniques for modifying and opening its band structure. To improve the anode performance, this research is using sulfur-doped reduced graphene oxide (S-rGO) layers. Sulfur-doped reduced graphene oxide (S-rGO) is typically synthesized through a two-step process. First, graphene oxide (GO) is prepared from graphite using chemical oxidation methods. Then, sulfur doping is achieved during the reduction of graphene oxide (GO) to reduced graphene oxide (rGO), where sulfur-containing compounds are introduced into the reaction mixture. Sulfur-doped reduced graphene oxide (S-rGO) can exhibit improved electrochemical properties, making it suitable for applications in energy storage devices such as lithium-sulfur batteries and supercapacitors. Using graphene as an anode material has a few advantages. Graphene has high electrical conductivity which facilitates efficient electron transport during the charging and discharging process. Graphene has a high surface area which can increase the electrode-electrolyte interface. This factor helps to enhance the specific capacity of the anode material. Unfortunately, pristine graphene has a low theoretical capacity for lithium storage which is why it needs to be functionalized with other elements like sulfur. Sulfur doping introduces defects and active sites on the graphene surface that can accommodate more lithium ions, which can increase the overall capacity of the anode material. Sulfur doping also can help to improve the reaction kinetics because it can help the diffusion of lithium ions and enhance

the reaction kinetics at the electrode-electrolyte interface. By functionalizing sulfur on the graphene, sulfur atoms can increase interlayer spacing between the graphene sheets and provide more room for lithium-ion intercalation, resulting in improved overall capacity and rate performance.

#### **1.4 Project Objective**

The main aim of this project is to develop a high-performance anode for LFP batteries using sulfur-doped reduced graphene oxide (S-rGO) layers. Specifically, the objectives are as follows:

- 1) To develop a lithium iron phosphate (LFP) coin cell battery using sulfur-doped reduced graphene oxide (S-rGO) layers as anode materials.
- 2) To evaluate the electrochemical performance of the LFP coin cells with S-rGO layers as anode materials through cyclic voltammetry (CV) and galvanostatic charge-discharge (GCD) testing.
- 3) To validate the performance and stability of the coin cell batteries by analyzing voltage, current, and power delivery over time using real-time data collected from a chassis car application.

#### **1.5 Scope of Project**

The scope of this project is as follows:

- a) Conducting a hydrothermal process to synthesize sulfur-doped reduced graphene oxide (S-rGO).
- b) Compositing the sulfur-doped reduced graphene oxide (S-rGO) with conductive additives and binders to prepare the anode electrode.
- c) Fabricating LFP coin cell battery under glove box conditions.

- d) Evaluating the electrical performance of the fabricated anode electrode in LFP coin cells via cyclic voltammetry (CV) and galvanostatic charge-discharge (GCD) testing.
- e) Validating coin cell battery performance and stability by measuring voltage, current, and power output through real-time data collection in a chassis car application.

## 1.6 Significant Research

Significant research is being done to improve the performance and durability of LFP batteries with sulfur-doped graphene anodes. These include developing optimized sulfur doping methods for graphene to improve lithium storage, conductivity, and stability, exploring alternative carbon-based anode compositions, and understanding lithium intercalation mechanisms at the atomic level. Electrode technology focuses on efficient architecture, nanostructures, and linkers to facilitate ion and electron transport. Electrolyte optimization includes new formulations, additives and solid or gel polymer electrolytes to improve conductivity, thermal stability, and safety. Computer modelling and simulations help predict the behaviour of materials, interfacial interactions, and performance under different conditions. Advanced characterization techniques elucidate structural, chemical, and morphological changes during cycling, enabling the analysis of degradation mechanisms and failure modes. Real-world testing, thermal management and system integration are critical to evaluating battery performance in electric vehicles and energy storage applications. Moreover, assessing the environmental impact, recyclability, and sustainable synthesis routes of graphene and other materials is crucial for the long-term viability of these battery systems.

## 1.7 Thesis Organization

The thesis is structured as follows: Chapter 1 begins by providing the research background and outlining the problem statement, objectives, and scope of the study. It emphasizes the importance of research, which focuses on synthesizing and functionalizing graphene by doping sulfur into the surface using a hydrothermal method. It also addresses the fabrication of a coin cell LFP and the analysis of its electrochemical performance through cyclic voltammetry technique.

Chapter 2 presents a literature review, summarizing previous studies and research on sulfur-doped reduced graphene oxide (S-rGO) and the various testing methods used in the field. Chapter 3 describes the methodology and experimental setup for validating the coin cell battery performance and its stability through real-time data collection from a chassis car application. The chapter details the analysis of key performance metrics including voltage profiles, current delivery, and power output to evaluate the batteries' operational characteristics under actual usage conditions. It also explains the testing methods employed in the study.

Chapter 4 analyses the data obtained from tests using the universal testing method and various materials. Finally, Chapter 5 presents the research's conclusions and provides recommendations for future studies in this area.

## CHAPTER 2

### LITERATURE REVIEW

#### 2.1 Introduction

Solar, wind, water, and geothermal heat are referred to as renewable energy. These sources are sustainable, and they do not contribute to greenhouse gas emissions or environmental deterioration during their extraction or consumption. Devices that use solar energy to change sunlight to either heat or electricity are called photovoltaic cells and solar thermal systems. Wind power that transforms the kinetic energy of the wind to electrical energy is used by wind turbines. For hydropower, turbines or dams are usually built to capture the energy of water moving in rivers and streams. Geothermal energy is often used for electricity generation and heating. It draws heat from beneath the surface of the Earth. Next, wood, agricultural residues, and waste, which are known as organic resources, can produce heat or electricity through combustion or conversion processes and are used via biomass energy. The growth of renewable energy plays a crucial role in mitigating climate change, fostering sustainable development, and reducing dependence on finite fossil fuels.

Unfortunately, due to the intermittent renewable energy sources, energy storage technology is needed to support the demand for electricity and other things. Energy storage is an essential part of overcoming the intermittent of renewable energy. Energy storage devices are designed to keep excess energy produced during the production process and release it during times of high demand or when electricity cannot be produced by renewable energy. One of the energy storage technologies is the battery. The battery is widely used in energy storage. They come in many types and sizes, such as coin cells, pouch cells, cylindrical cells, and prismatic cells. It can be found in electronic devices for massive

installation, or these batteries also can be found in grid-scale applications. In the end. The need for energy storage to support renewable energy technologies is needed as efficient energy storage technology speeds up the shift to a more robust energy system. It is because these technologies can enhance grid stability and energy efficiency and enable greater integration of renewable energy. In this chapter, the development of the anode materials is explained in detail to overcome the battery's limitation.

## **2.2 Lithium-Ion Battery (LIB)**

Lithium-ion batteries (LIBs) are known as rechargeable power cells. Currently, the LIB is one of the most promising energy storage systems because of its outstanding electrochemical performance and high capacity [3]. LIBs are used in many sectors, ranging from handheld electronics to large-scale energy reserves. With their capability to undergo many recharge cycles, diminished propensity for self-discharge, and elevated energy density, these LIBs are gaining popularity abruptly among people. LIBs are being used in various fields as energy storage technology keeps growing to meet the high demand in human life.

The fundamental structure of a LIB includes three primary components, which are a positive electrode, a negative electrode, and an electrolyte. Typically, the negative electrode, called the cathode, incorporates lithium metal oxide compounds like lithium nickel manganese oxide (NMC), lithium iron phosphate (LFP), and lithium manganese oxide (LMO). For the positive electrode, it is known as anode. The anode materials usually consist of graphite. Next, the electrolyte is commonly composed of lithium salt dissolved within an organic solvent that will ease the transport of lithium ions during charging and discharging cycles.

LIBs maintain their position in the market segments of electronic devices, electric vehicles, and energy storage infrastructure. The popularity of these batteries is driven by

their performance metrics, scalability, and well-established manufacturing capabilities. Importantly, ongoing research and development of LIBs are actively addressing the limitations of lithium-ion technology and exploring all the alternatives to enhance battery chemistry and material compositions. This continuous innovation is crucial to align with the high demand for sustainable and effective energy storage systems. Figure 2.1 below illustrates the diverse applications of LIBs.

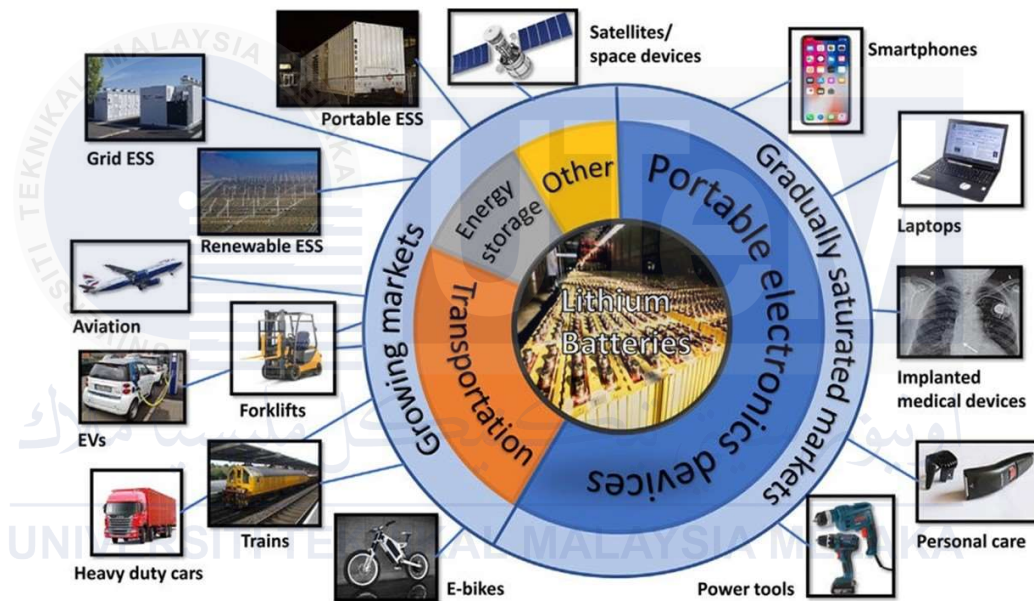


Figure 2.1: Applications of Lithium-Ion Battery

### 2.2.1 Type Of Lithium-Ion Battery (LIB)

LIBs have emerged as versatile solutions for energy storage that exhibit a wide range of types, shapes, and sizes to cater to diverse applications. These batteries are available in various forms, including coin cells [4], pouch cells [5], cylindrical cells [6], and prismatic cells [7], each designed to meet specific requirements. The several types of LIBs are

perfected for distinct performance characteristics, such as energy density, power density, safety, and cost-effectiveness. This inherent flexibility in LIBs allows manufacturers to select the most suitable type for their products, ensuring the best performance and efficiency. In this way, the wide range of LIB types available in the market enables the widespread adoption of this technology across various industries, ranging from consumer electronics to electric vehicles and energy storage systems.

Firstly, there is the lithium nickel manganese oxide (NMC) battery, a type of LIB. This battery is made from a combination of nickel, manganese, and cobalt, with the specific ratios of these elements varying to achieve a balance between energy density, life cycle, and power capability. NMC batteries are known for their improved cycle life, thermal stability, and higher energy density compared to other LIBs. Tran M and friends state in their studies that NMC uses a different cathode material compared to the commonly used LFP (Lithium Iron Phosphate) [8]. Unlike LFP, which is known for its good capacity and stability, NMC batteries offer improved cycle life, thermal stability, and higher energy density. The cathode in NMC batteries has a layered structure and undergoes a single-phase intercalation process during charge and discharge cycles, in contrast to the olivine structure found in LFP batteries. The discharge chemistry of NMC batteries is similar to LFP batteries, as they are both lithium-ion batteries.

Next, lithium manganese oxide (LMO) batteries are one of the kinds. Referring to research conducted by Lu. J, the spinel LMO has garnered significant attention due to its notable advantages, including abundant precursors, low cost, environmental friendliness, high working voltage, and intrinsic thermal stability [9]. Compared to other cathode materials, LMO features an open three-dimensional lithium diffusion pathway that facilitates the insertion and extraction of lithium ions. However, its rate capability remains poor due to low electronic conductivity and slow lithium-ion diffusion, thereby limiting its applicability

in high-power lithium-ion batteries. Although nanostructured LMO materials have been explored to mitigate these challenges, they encounter issues such as low tap density and unstable, complex fabrication. Porous micro-sized LMO particles have the potential to strike a balance between favourable rate capability and high tap density, yet limited research has achieved high-rate capabilities exceeding 20C with these materials.

Lastly, the other type of LIB is the lithium iron phosphate ( $\text{LiFePO}_4$ ) battery. Yue research shows that  $\text{LiFePO}_4$ , with its olivine structure comprising phosphate-oxygen tetrahedra, iron-oxygen octahedra, and lithium-oxygen octahedra, is lauded as an excellent cathode material for LIBs due to its high energy density (170 mAh/g), smooth discharge plateau, exceptional cycling and thermal stability, and low raw material costs [10]. The strong covalent bonds between phosphorus and oxygen enhance safety and cycling endurance. However, the separation of iron-oxygen octahedra by phosphate anions hinders a continuous iron-oxygen network, resulting in low electronic conductivity ( $10^{-9}$  to  $10^{-10}$  S/cm) and lithium-ion diffusion coefficient ( $D_{\text{Li}} < 10^{-14}$  cm<sup>2</sup>/s), limiting its rate performance for high-discharge power batteries. For these applications, lithium iron phosphate ( $\text{LiFePO}_4$ ) batteries are the best type of lithium-ion batteries that can be used with the best performance compared to others [10].

These examples are just a few variations of LIB. Numerous combinations of materials are used to achieve specific performance for different applications. When selecting the right battery, it is important to consider factors such as energy density, life cycle, cost, power requirements, and safety in order to optimize the performance of the systems or applications where the battery will be used. Understanding the specific requirements and operating conditions will help in choosing the most suitable lithium-ion battery for the intended application. It is important to stay updated with the latest advancements and innovations in lithium-ion battery technology to make informed decisions and benefit from

improved performance and safety features. The continuous research and development in this field offer promising prospects for enhanced battery technologies that can meet the evolving needs of various industries and applications.

### **2.2.2 Lithium Iron Phosphate (LFP) Battery**

Lithium Iron Phosphate (LFP) batteries, also referred to as LFP batteries, are gaining significant attention and adoption nowadays. LFP batteries are one of the LIBs that are usually used in applications that prioritize safety, longevity, and stability. It is widely used on electric vehicles LIBs since the LFP cathode is relatively stable and safe, or to put it another way, more dependable under complex operating conditions. Lithium iron phosphate ( $\text{LiFePO}_4$ ) is used as the cathode material in the battery, while carbon-typed materials are used as the anode. Typically, the electrolyte used in this type of battery is the lithium salt dissolved in an organic solvent. LFP batteries use iron as the transition metal in cathode material, unlike the other lithium-ion batteries chemistry that contains nickel, manganese, or cobalt. By using iron as the transition metal in the cathode material, it helps to enhance their stability and safety characteristics.

These types of batteries are famous because one of the advantages is their inherent safety, where they are less prone to thermal runaway, which is the phenomenon where the battery's temperature uncontrollably increases, which will lead to explosions or fires. LFP batteries have a very stable crystal structure that is hard to break down even when overcharging conditions occur. To further enhance their safety, this battery is less reactive with air and moisture than other LIBs. Additionally, LFP batteries can withstand a high number of charge-discharge cycles. It exhibits a longer life cycle without much degradation in the battery's performance. With a robust crystal structure, this battery is well-suited for

any applications and technologies where longevity and reliability are crucial like stationary energy storage systems and so on.

Next, LFP batteries are gaining attention in various fields because of their stability. With excellent chemical and thermal stability, they can overcome various accidents that occurred especially during elevated temperatures, over-discharge and overcharging conditions that result in reducing the risks of any hazard happening. This battery also has a lower energy density compared to other LIBs. With an advanced electrode design, the energy density of the battery can be improved and make it suitable to be used in a wide range of operating conditions and the demand is surprisingly increased in various markets.

LIBs are extensively used in electric vehicles, backup power supplies, and portable electronics due to their exceptional safety, longevity, and stability. Among these qualities, LFP batteries stand out, particularly in applications where reliability and safety are crucial. Their widespread use is a testament to their effectiveness and dependability in various fields. These batteries have proven to be a reliable and safe choice, making them highly sought after in the market. The exceptional performance of LFP batteries makes them a preferred option for applications where safety and longevity are top priorities. Their widespread adoption in different industries is a testament to their superior performance and reliability. Figure 2.2 below shows an example of an LFP battery in a coin cell shape.

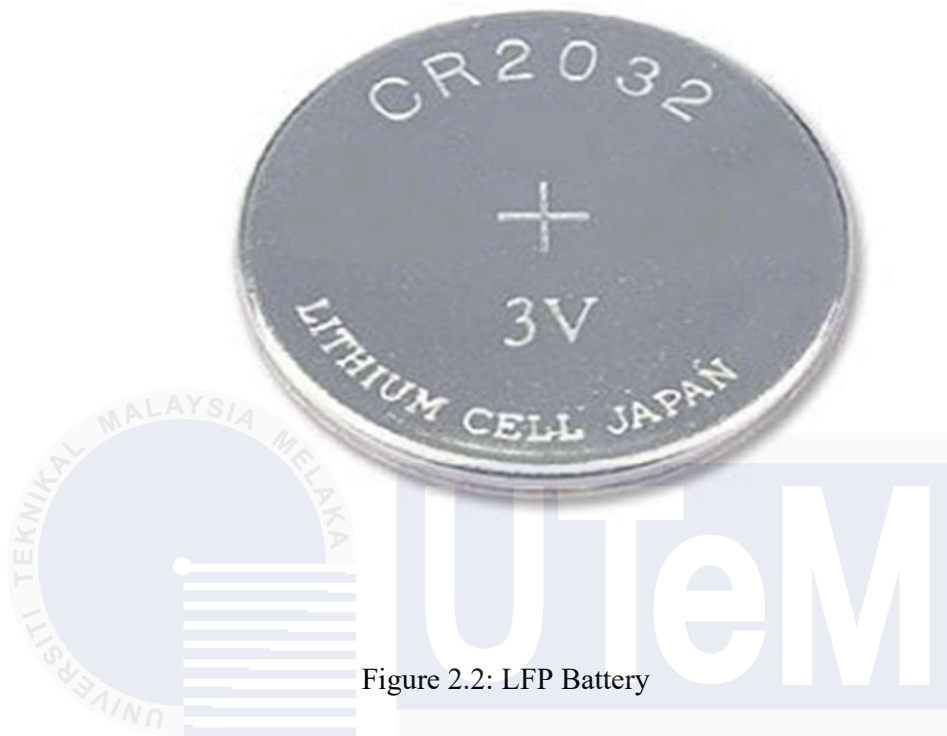


Figure 2.2: LFP Battery

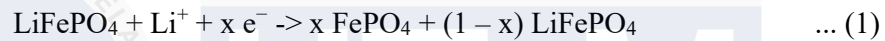
### 2.3 Mechanism of LFP

The lithium iron phosphate (LFP) working principle involves a few electrochemical reactions that will occur within the battery's components during the charging and discharging cycles. It consists of three main components, which are the cathode, which is made of lithium iron phosphate itself; the anode, which is usually composed of carbon; and the electrolyte solution, which contains lithium ions ( $\text{Li}^+$ ). A porous membrane works as a separator that separates the anode and cathode while allowing the lithium ions to flow through the electrolyte without mixing the electrodes.

During the charging process, an external power source will apply a voltage across the battery terminals. Lithium ions ( $\text{Li}^+$ ) will be absorbed into the cathode material and increase the lithium content in the electrode to make sure that it can be ready to be used. But

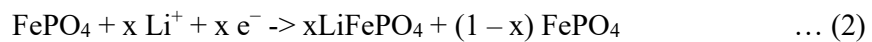
at the anode electrode, lithium ions ( $\text{Li}^+$ ) are released back into the electrolyte to complete the cycle of lithium ions movement between the cathode and anode to generate electrical energy. The electron flows through the electrolyte from the anode to the cathode during the charging process. During the charging process, lithium ions ( $\text{Li}^+$ ) are removed from the cathode to give iron phosphate ( $\text{FePO}_4$ ) as shown in Equation (1) [11]. With the completion of electron flows, the battery can store the electrical energy generated and it will be ready to be used when needed.

Equation 1



As the battery discharges the energy stored, lithium ions ( $\text{Li}^+$ ) are released from the cathode and flow through the electrolyte towards the anode. At the anode electrode, lithium ions ( $\text{Li}^+$ ) are absorbed into the carbon material. In the discharging process, the route is inverted with the insertion of Li into  $\text{FePO}_4$ , as shown in Equation (2) [11]. This process causes the anode electrode to become negatively charged during the discharging process. Electron flow will be reversed, unlike the flow during the charging process. When lithium ions ( $\text{Li}^+$ ) travel from cathode to anode, electrons will flow through the external circuit and generate electricity that can be used for the connected device or applications. The generated electrical energy also can be stored for later use in various applications.

Equation 2



### 2.3.1 Battery Structure

There are several key components in the structure of an LFP battery that are composed and arranged in specific arrangements to make sure the necessary electrochemical reactions in the battery are being processed, whether it will store or release the energy. The battery structure contains an anode as the negative electrode, a cathode as the positive electrode, an electrolyte, a separator, and, lastly, the container or casing (Figure 2.3). All the components need to be assembled in the battery to make sure the battery can function properly.

First, the positive electrode, which is the cathode, is made of lithium iron phosphate ( $\text{LiFePO}_4$ ) particles that will be embedded in a conductive matrix. Particles are compounds that reversibly intercalate the lithium ions during charging and discharging cycles. To enhance the electron transfer and to improve the conductivity of the cathode, conductive additives like carbon black usually will be mixed with lithium iron phosphate ( $\text{LiFePO}_4$ ) particles. The current collector for the cathode, aluminium foil, is commonly used because it can provide a pathway for electrons to travel out of the battery during the discharge process.

Secondly, a negative electrode, known as an anode, is typically made of carbon-based materials such as graphite, carbon black and so on because this type of material is capable of intercalating lithium ions during charging accordingly. The anode also has conductive additives and coated onto a current collector similar to the cathode, but in the anode, the current collector that usually being used is the copper foil. In addition, this battery has a separator that is assembled to prevent direct contact between the anode and cathode. The separator is a porous membrane that is placed between those two electrodes. It will prevent short circuits, but at the same time, it will allow the lithium ions to flow through.

Commonly, the separator materials used are microporous polyethylene or polypropylene films that have a high electrolyte permeability and mechanical strength.

Following this, another vital component in the battery is the electrolyte and the container or casing. The electrolyte is a solution that contains lithium salts dissolved in a solvent which is made from a mixture of organic carbonates. It serves as the medium for the ions to transport from the cathode to the anode during the charging and discharging process. Generally, the lithium salts used in electrolytes include lithium hexafluorophosphate ( $\text{LiPF}_6$ ) and lithium tetrafluoroborate ( $\text{LiBF}_4$ ). Next is the casing of the battery. All the battery components are housed in a casing that is made of metal or plastic. It will provide mechanical support, the insulation of the electrical, and protection against any external impacts and environmental conditions. It will also include the terminals for connecting the battery to any devices or external circuit in any application.

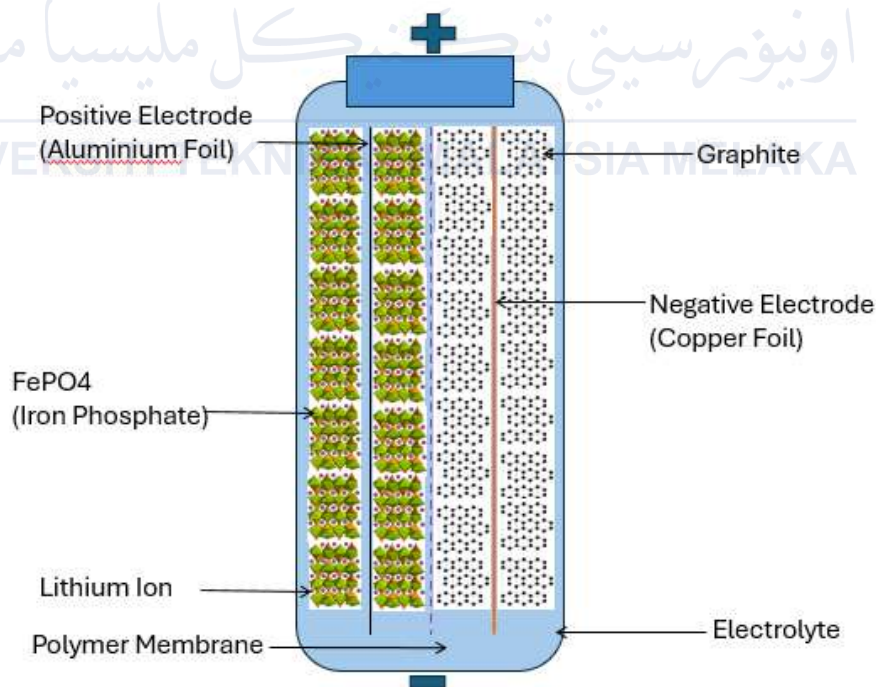


Figure 2.3: LFP Battery Structure

### 2.3.2 Comprehensive Review of Anode Materials

Graphite is one of the most used materials for anodes in LIBs. Graphite is a form of carbon that comes in a layered structure where the atoms are arranged in stacked sheets. Each one of the sheets consists of a hexagonal lattice of carbon atoms bonded together, resulting in a strong covalent bond within the plane. The interaction between adjacent layers is relatively weak to make sure that intercalation of lithium ions between layers during the charge-discharge cycle can be allowed. Graphite's specific capacity is around 372 mAh/g which means it can store around 372 milliampere-hours of charge per gram of the material. Graphite shows a great balance of specific capacity, cycling stability and cost-effectiveness with lower specific capacity than other potential anode materials. The replacement of graphite (with a theoretical specific capacity of 379 mAh/g) as an anode for a material with higher capacity is being researched, driven by the electric vehicle (EV) demand [12]. Typically, graphite can exhibit excellent cycling stability and potentially allow thousands of charge-discharge cycles with minimal capacity fade. With the robustness of the structure and the ability of reversible nature of lithium intercalation, graphite can prevent significant structural degradation over repeated cycles, but it still can experience capacity loss over time due to a few factors like solid-electrolyte interphase (SEI) formation and electrode-electrolyte interactions.

Additionally, graphite brings a lot of benefits as it is used as an anode material. Graphite has excellent electrical conductivity. By using graphite, the rapid movement of the electrons is smoother during charge-discharge cycles, improving the efficiency of the battery. It is also abundant, making it one of the most cost-effective materials in production. With its good mechanical stability, it can maintain the integrity of the structure even if it goes under multiple processes. Graphite also does not readily react with the battery components and the electrolyte because it is chemically inert. This helps to increase the

safety and reliability of the battery during its operation. But graphite itself comes with low energy density and limited specific capacity. These factors may restrict the performance of the batteries to fully operate, and these limitations actually lead to some research that aims to improve and explore alternatives to increase graphite's performance as an anode material.

One more potential anode material other than graphite is metal oxides such as Tin dioxide ( $\text{SnO}_2$ ), Titanium dioxide ( $\text{TiO}_2$ ), Manganese dioxide ( $\text{MnO}_2$ ), and other metal oxides. Jung and others have done research about tin dioxide ( $\text{SnO}_2$ ), and they stated that tin dioxide ( $\text{SnO}_2$ ) is a promising material for lithium-ion battery anodes due to its high theoretical specific capacity, safe working potential, low cost, and environmental friendliness [13]. However, its practical use is limited by pulverization during alloying and dealloying, leading to loss of electrical contact and the formation of an unwanted solid electrolyte interphase (SEI). To address these challenges, those researchers have explored methods such as Nanostructuring and compositing with carbonaceous materials.

Next, another metal oxide that has been grabbing attention is titanium oxide. Madhusanka has studied  $\text{TiO}_2$  as one of the anode materials that can be used in LIB [14]. While tin (Sn) and silicon (Si) have been extensively studied as anode materials due to their high energy density, they suffer from issues such as large volume expansion during charge-discharge processes, significant irreversible capacity loss, and poor cyclability.  $\text{TiO}_2$ , with its various electrochemically active forms (anatase, rutile, brookite, and  $\text{TiO}_2(\text{B})$ ), has been widely researched in recent years due to its superior properties, such as high operating potential ( $\sim 1.75 \text{ V vs. Li/Li}^+$ ), chemical and mechanical stability even at high current rates (C-rates), low volume expansion ( $< 5\%$ ) during Li insertion-disinsertion processes, low cost, and eco-friendliness. However,  $\text{TiO}_2$ 's practical application in LIBs is severely hindered by its significant drawbacks, such as poor electronic conductivity ( $10^{-13} \text{ Scm}^{-1}$ ) and low lithium-ion diffusion ( $10^{-10} - 10^{-17} \text{ cm}^2 \text{ s}^{-1}$ ).

Manganese oxide is also one of the metal oxides being explored as an anode material in LIBs. Choi reported that manganese oxides ( $\text{MnO}_2$ ) offer several advantages over other transition metal oxides (TMOs) as anode materials for LIBs [15]. These advantages include a lower equilibrium potential in the forward reaction and a smaller voltage hysteresis between forward and reverse reactions. However, it has been difficult to extract the theoretical capacity of  $\text{MnO}_2$  with stable cycling performance due to its low electronic conductivity ( $\sim 10^{-7}$  to  $\sim 10^{-8}$   $\text{S cm}^{-1}$ ), large volume changes, and diffusion-induced stresses resulting from significant structural changes during the conversion reaction. Recent studies indicate that the theoretical capacity of  $\text{MnO}_2$  can be achieved by reducing its size to the nanoscale and combining it with conducting substrates like carbon. Porous and nanostructured  $\text{MnO}_2$  composites with carbon are preferred for achieving high capacity and long cycle life.

There is a significant amount of ongoing research aimed at enhancing and optimizing materials for use in LIBs. Each material has its own distinct set of advantages and challenges, and researchers are actively working to improve their performance for practical application in LIBs. This involves studying the properties of various materials, such as graphite/graphene and metal oxides like tin oxide ( $\text{SnO}_2$ ), titanium oxide ( $\text{TiO}_2$ ), manganese oxide ( $\text{MnO}_2$ ) and so on to understand how they can be optimized to enhance battery performance. By delving into the intricacies of these materials, scientists hope to address issues such as energy density, cycle life, and safety, ultimately paving the way for more efficient and reliable lithium-ion battery technologies. The outcomes of this research could lead to significant advancements in energy storage, benefiting a wide range of applications from portable electronics to electric vehicles.

## 2.4 Graphene as Anode Materials

Graphene is a two-dimensional single layer of carbon arranged in hexagonal order, which is a conductive substrate being widely researched with its potential to make high-performance lithium-ion batteries [16]. Graphene is one of the materials that can be used as anode material in LFP batteries. Graphene is one of the remarkable materials composed of a single layer of carbon atoms. It is arranged in a two-dimensional honeycomb lattice. It gained attention in various fields because of its special characteristics, such as high electrical conductivity and thermal conductivity, flexibility, mechanical strength, and transparency. These properties make graphene one of the popular and potential candidates for various uses in various fields like in electronics, biomedical devices, and energy storage systems.

In LFP batteries, graphene plays crucial work as an additive to improve the performance of the battery. LFP batteries are famous for their stability, long life cycle and many more but they suffer from low electrical conductivity that limits their rate capability and overall performance. Graphene is being used in LFP batteries to improve electrical conductivity by adding it to the electrodes. Both ions and electrons' movement can be smoother resulting in better performance where the charge-discharge rate can be increased. With graphene's high surface area, it potentially improves the energy density of the battery where active sites as provided more.

Next, graphene can be synthesized in many ways. Firstly, graphene can be synthesized through mechanical exfoliation where the layers of graphite will be peeled off by using the adhesive type. The exfoliation will be continuous until the layers of graphite become a single-layer graphene. The second one is chemical vapor deposition (CVD), also known as one of the ways to synthesize graphene. A carbon-containing gas is being introduced into a high-temperature furnace along with substrate materials like copper or silicon dioxide. This method can be used when large-area graphene needs to be synthesized.

Chemical reduction of graphene oxide is one of the methods to synthesize graphene. Graphene oxide can be synthesized through the chemical oxidation of graphite flakes, but then it can be reduced back to its initial form, graphene, by using thermal or chemical methods where oxygen-containing functional groups need to be removed, and this method can be beneficial for certain applications.

Graphite needs to be functionalized to overcome its inherent limitations and customize its properties for various applications. This process weakens the interlayer van der Waals forces, allowing it to be separated into graphene sheets. It also adds hydrophilic groups to improve solubility and processability using solution-based methods. These functional groups alter the surface properties, improve compatibility with other materials in composites, and create active sites for further reactions or immobilization. Covalent functionalization can adjust the electronic structure, enhance conductivity, and improve mechanical properties through interfacial interactions or cross-linking. Overall, functionalization broadens the potential applications of graphite or graphene in fields such as composites, electronics, energy storage, and catalysis by addressing the limitations of pristine graphite and customizing its properties.

#### **2.4.1 Type of Functionalized Graphene**

Graphene needs to be functionalized. Unfortunately, one serious challenge in using graphene as a conductive material in LIBs is that the planar structure of graphene shows a steric hindrance effect for lithium-ion diffusion [1]. So, the graphene needs to be functionalized and functionalized graphene can be achieved by adding functional groups or molecules into it. This action can change graphene's characteristics, enhancing its compatibility with diverse materials. Functionalizing graphene is being conducted to improve graphene's dispersion in solvents or matrices. It also helps the integration of

graphene with polymer matrices. Introducing the functional groups to graphene can strengthen the bond between graphene and polymers, resulting in improved composite performance, and functionalizing enables precise tuning of graphene's electronic properties. It broadens graphene's applicability across various fields by adjusting its properties to meet the demands of specific requirements. There are a few types of functionalized graphene, such as graphene oxide, reduced graphene oxide like sulfur-doped reduced graphene oxide and heteroatom-doped graphene.

#### **2.4.1.1 Graphene Oxide (GO)**

Graphene oxide (GO) is one of the derivatives of graphene. Graphene is a two-dimensional (2D) material made from monolayer graphite with honeycomb structure. Its low cost and ease to synthesize are other reasons why GO has great interest [17]. Graphene contains the oxygen functional groups attached to the basal plane and edges known as graphene oxide (GO). By using strong oxidizing agents like sulfuric acid, potassium permanganate or nitric acid, this type of graphene can be produced. The material produced will be like graphene, which consists of a single or few layers of carbon atoms in a honeycomb lattice shape, but it contains a significant number of oxygen-containing functional groups. Compared to pristine graphene, graphene oxide has several unique properties thanks to those oxygen functional groups. Due to the abundance of hydroxyl and carboxyl, graphene oxide is highly hydrophilic and makes it dispersible in water and other polar solvents.

Those oxygen functional groups introduce defects that disrupt the  $sp^2$  carbon network of graphene and help to increase the bandgap compared to pristine graphene. With the increases in the bandgap, tenability can be allowed. Like pristine graphene, graphene oxide also has good mechanical properties, but the presence of the functional groups makes

the structure sit in disorder conditions where it can reduce the electrical conductivity compared to pristine graphene. The electrical conductivity of graphene oxide can be restored through the reduction process and become the reduced graphene oxide (rGO) without disturbing the functionalized graphene's advanced properties.

#### **2.4.1.2 Reduced Graphene Oxide ( rGO )**

Graphene oxide that undergoes a reduction process is referred to as the reduced graphene oxide (rGO). It goes under a reduction process to drop the oxygen functional groups in graphene oxide. This rGO is usually obtained by the reduction of graphene oxide (GO), which means the need for an extra reducing agent (like toxic hydrazine) or more thermal annealing process [18]. It will involve thermal, electrochemical, or chemical treatment as the graphene oxide goes under the reduction process. This process is being conducted to restore the  $sp^2$  carbon network characteristic of the pristine graphene. There will be a few changes in graphene oxide properties. Basically, the reduction of the graphene oxide will improve the electrical conductivity of the graphene oxide. It will grow in potential, especially in applications that require conductive materials such as electrodes in the battery, electronic devices, and sensors.

The bandgap of the graphene oxide will be reduced with the reduction of its bandgap. The rGO properties will be similar to pristine graphene. Additionally, mechanical properties like the strength and flexibility of the graphene oxide can be improved as graphene oxide undergoes the reduction process compared to many other materials. This shows that reduced graphene oxide is a versatile material that comes with various applications in diverse fields, including energy storage systems, electronics, sensors, and biomedical devices. It is one of the materials that potentially grow in the market of practical applications in various fields.

### 2.4.1.3 Sulfur-doped Reduced Graphene Oxide ( S-rGO )

Sulfur-doped reduced graphene oxide (S-rGO) is a material derived from the reduction of graphene oxide where sulfur atoms are added to the structure of the graphene. To produce sulfur-doped reduced graphene oxide, a few processes need to be carried out. Firstly, graphene oxide itself needs to be synthesized by adding those functional groups that contain oxygen to the graphene. By oxidizing the graphene with strong oxidizing agents like sulfuric acid and so on, graphene oxide can be obtained. Secondly, the graphene oxide obtained needs to undergo a reduction process to remove some portion of the oxygen-containing functional groups. This step will help the graphene to restore the conjugated  $\pi$ -electron system, and the electrical conductivity can be improved.

Lastly, the most crucial step is sulfur doping. This process can be done during the reduction process, or it can be done separately where a sulfur-containing precursor will be introduced to reduced graphene oxide. The sulfur atoms will be added to the graphene lattice and substitute the carbon atoms in the graphene. Sulfur-containing functional groups will be formed on the graphene's surface and this process will help the graphene's performance to increase. By doping the sulfur to the reduced graphene oxide, it can enhance the electrical conductivity and increase the active surface area of the graphene. Sulfur atoms will provide more charge carriers and improve the electron transport properties. In this doping process, sulfur will introduce defects and structural distortions in the graphene lattice and then increase the active surface area, which can help to create more catalytic reactions and electrochemical processes.

## 2.5 Electrochemical Performance

Electrochemical performance is being carried out because it is crucial for their life span, stability, and safety evaluation. By evaluating the LIB electrochemical performance, the design and materials used in the battery can be optimized to improve overall performance. Electrochemical performance will help researchers identify the potential issues that are related to the capacity fade, thermal stability, and power capability. Better charging protocols and battery management systems can be developed to extend battery life is one of the reasons why electrochemical performance is evaluated. Voltage features, current density distribution, electrochemical impedance, electrolyte concentration distribution and cycling performance will be studied to gain more understanding of the battery's behavior and the degradation mechanism.

There are a few methods that can be used to evaluate the electrochemical performance of the battery. The first method used in this study is cyclic voltammetry (CV), where the potentially working electrode is linearly swept between two values at a fixed scan rate, and the resulting current is measured. As the potential between the two electrodes is swept back and forth, the chemical species undergo oxidation or reduction by losing or gaining electrons, respectively. Usually, the scan rate used in CV typically ranges from 10 mV/s to 1000mV/s. This value depends on the specific system that is being studied. This technique provides key insights into the redox behaviour, reaction kinetics, concentration, and surface properties of the electroactive analytes present. It allows studying the thermodynamics of redox processes, determining energy levels of species, and probing the kinetics of electron transfer reactions.

Next, galvanostatic charge-discharge cycling is a widely used technique to evaluate battery performance, especially for LIBs. During these cycles, the battery undergoes charging and discharging at a constant current rate called the galvanostatic rate. In the

charging phase, a fixed current flows into the battery until reaching a specified maximum voltage limit. This allows ions to move and energy to be stored as chemical potential within the battery. Conversely, in the discharging phase, the battery provides a constant current output until hitting a minimum voltage cutoff. This releases the stored chemical energy as electrical power to operate devices or systems.

### 2.5.1 Cyclic Voltammetry (CV)

Cyclic voltammetry is an electrochemical method that characterizes redox-active (oxidation-reduction) species in solution by cycling the applied potential linearly and measuring the resulting current response. As studied by Chen conducted cyclic voltammetry methods in their research [19]. The CV curves of a 65% Si nanoparticles/35% graphene composite electrode exhibited key features related to lithiation/de-lithiation processes. The first lithiation half-cycle showed a peak around 0.75V attributed to solid-electrolyte interphase (SEI) formation, explaining the low initial coulombic efficiency. Subsequent cycles had a peak near 0.15V ascribed to lithium-silicon alloying. Anodic peaks at 0.37V and 0.55V corresponded to phase transitions between lithium-silicon alloys and silicon during de-lithiation. The de-lithiation peak intensities gradually increased from the 1st to 5th cycle, attributed to the progressive breakdown of the silicon structure as shown in Figure 2.4(a). This breakdown depended on the lithium migration rate into silicon and the rate of amorphous lithium-silicon alloy formation.

In a second study by Fan, cyclic voltammetry (CV) measurements at different scan rates (0.1-0.5 mV/s) were analysed to study the conversion redox kinetics of lithium polysulfides (LiPSs) and calculate lithium-ion ( $\text{Li}^+$ ) diffusion coefficients [20]. In their studies, the peak currents in the CV curves showed a linear relationship with the square root of the scan rates. Higher peak currents and steeper slopes corresponded to faster  $\text{Li}^+$  diffusion

kinetics. In addition, they stated that due to rapid  $\text{Li}^+$  diffusion, the SCF@rGO/S cathode had a high electronic conductivity of 4.64 S/cm compared to 2.73 S/cm for SCF/S and 0.22 S/cm for PPC/S electrodes. The high conductivity of SCF@rGO/S enhanced ion-electron interactions facilitated redox reactions and reduced polarization during the electrochemical process. Figure 2.4(b) shows the results of the electrochemical performance that they have done.

Additionally, cyclic voltammetry tests were performed on sulfur-carbon composites using a BCS Biologic instrument by Venezia. The tests were conducted at a scan rate of 0.1 mV/s over the potential range of 1.7-2.8 V [21]. From the CV data, the lithium-ion diffusion coefficient was figured out using the Randles-Sevcik equation. The CV profiles displayed the typical multi-step lithium-sulfur reaction behaviour. An initial reduction peak at around 2.3 V indicated sulfur reduction to long-chain polysulfides, followed by a peak at 1.9-2.0 V for the formation of shorter polysulfides (Figure 2.4(c)). The anodic peaks at 2.3-2.4 V suggested oxidation back to higher order polysulfides and sulfur. Samples with  $\leq 70$  wt% sulfur showed a higher current peak for the 2.3 V reaction, while  $>70$  wt% sulfur showed a higher 2.4 V peak. This difference was attributed to varying extents of complete polysulfide-to-sulfur conversion based on the sulfur content.

Furthermore, Tite and friends have done cyclic voltammetry measurements, and it were recorded at room temperature using an Origaflex-OGF05A system within the 2.0V – 4.0V voltage range, at a scan rate of 0.1 mV/s [22]. They show that cyclic voltammetry measurements on G/Al,  $\text{V}_2\text{O}_3/\text{G}/\text{Al}$  and Sn- $\text{V}_2\text{O}_3/\text{G}/\text{Al}$  electrodes between 2.0-4.0 V vs  $\text{Li}/\text{Li}^+$  at 0.1 mV/s scan rate showed similar behaviour in the first three cycles with no major irreversible processes (Figure 2.4(d)). The vanadium oxide samples exhibited small redox peaks related to multi-step lithium intercalation/deintercalation, with low peak intensities attributed to the nanomaterials' high surface area. Sn-doping in  $\text{V}_2\text{O}_3$  reduced the potential

differences between reduction and oxidation peaks, indicating improved lithium intercalation/deintercalation kinetics compared to undoped  $V_2O_3$ . The CV curve areas represent the total stored charge from electric double-layer capacitance and faradaic processes [22].

Lastly, by referring to Guan research, in their study, they used cyclic voltammetry (CV) measurements with scan rates ranging from 0.01 to 1.0 mV/s to analyse the kinetics of lithium-ion (de)intercalation [23]. When examining pure GA, the initial CV showed a broad cathodic peak at around 0.2 V, which was attributed to the formation of the solid electrolyte interphase (SEI). Additionally, a cathodic peak at approximately 0.01 V indicated the Si-Li alloying reaction and a broad anodic peak below 1.5 V corresponded to the de-lithiation of  $Li_xSi$ . In subsequent scans, only the cathodic peak at around 0.01 V and the anodic peak below 1.5 V appeared, demonstrating a reversible reaction as shown in Equation 3. In the case of GA-G-2-1, they observed the same peaks, along with an additional anodic peak at approximately 0.16 V related to graphene de-lithiation, which persisted in later CV cycles [23]. The CV results obtained at different scan rates provided valuable insights into the kinetics of lithium intercalation and deintercalation in these silicon/graphene composite anodes as illustrated in Figure 2.4(e).

Equation 3



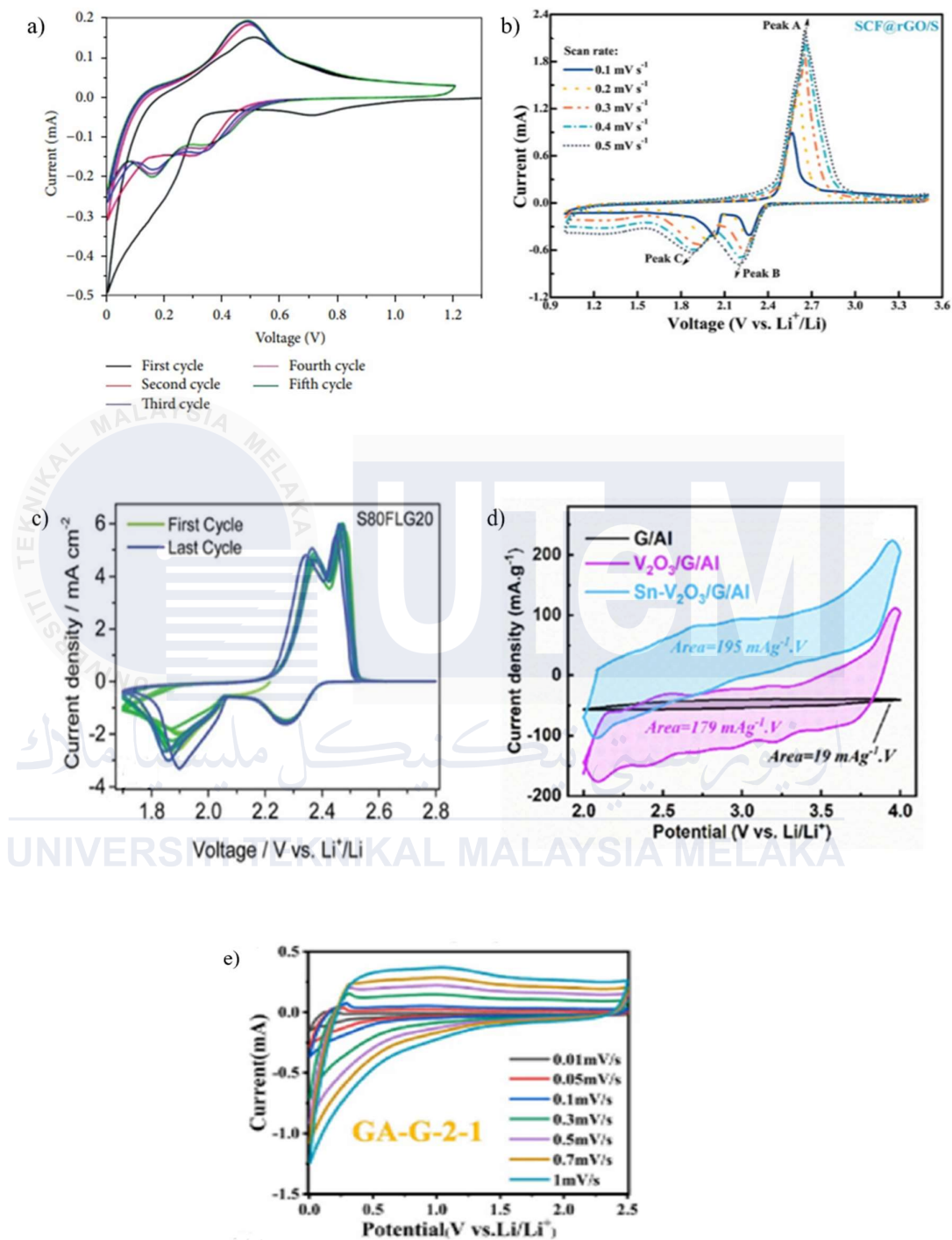


Figure 2.4: (a) The CV curves of 65% Si nanoparticles/35% graphene composite,  $V = 0.1 \text{ mV/s}$ . 1st to 5th cycle [19]. (b) SCF@rGO/S at various scan rates [20]. (c) CV tests of the S80FLG20 [21]. (d) CVs at the scan rate of  $0.1 \text{ mV s}^{-1}$  up to three cycles and estimation of the area under the CV curves [22]. (e) CV curves of Pure GA and GA[1]G-2-1 at different scan rates [23].

## 2.5.2 Galvanostatic Charge-Discharge (GCD)

Galvanostatic charge-discharge (GCD) is a widely utilized technique for characterizing the electrochemical performance of energy storage devices, such as supercapacitors and batteries. It involves applying a constant current to charge and discharge the device while monitoring the potential response. The GCD method offers several advantages, including direct information about capacitance, energy density, power density, and insights into charge storage mechanisms and kinetics. During a typical GCD experiment, a constant current charges the device until reaching a set upper potential limit, followed by reversing the current to discharge until a lower potential limit. The specific capacitance, energy density, and power density can be calculated from the GCD curve using established equations such as shown in Equations 4, 5 and 6 respectively [24]. GCD experiments at different current densities assess rate capability and charge storage kinetics, while the curve shape provides a mechanistic understanding of capacitive or battery-like charge storage processes. Overall, GCD is an essential tool for evaluating and optimizing the performance of supercapacitors and batteries, enabling direct quantification of key parameters and mechanistic insights.

$$C = \frac{1 \int V dt}{m (V_f - V_i)^2} \quad (\text{Equation 4})$$

$$E = P \times \frac{t}{3600} \quad (\text{Equation 5})$$

$$P = \frac{I \times \Delta V}{m} \quad \text{where } \Delta V = \frac{(V_f - V_i)}{2} \quad (\text{Equation 6})$$

By referring to research that has been done by HE, the test parameters involved GCD with an initial potential of 3.0 V and an end potential of 0.01 V (vs Li/Li<sup>+</sup>) [25]. The GCD tests were conducted at 100 mA/g for 100 cycles as shown in Figure 2.5(a). The initial discharge capacity was 1460 mAh/g with 57.9% coulombic efficiency due to solid electrolyte interphase formation and electrolyte decomposition. From the 5th cycle onwards,

coulombic efficiencies exceeded 98%, and capacity retention was 91.1% after 100 cycles. In contrast, pure MoS<sub>2</sub> anode exhibited an initial discharge capacity of 338.1 mAh/g, increasing to over 800 mAh/g before fading to 256 mAh/g after 75 cycles. The MoS<sub>2</sub>/graphene anode demonstrated excellent reversibility with well-overlapped charge-discharge profiles from the 3rd cycle [25]. Long-term cycling at 1000 mA/g showed remarkable durability with 901.8 mAh/g capacity and 98.9% retention after 700 cycles. Rate capability tests revealed high reversible capacities of 992-1067 mAh/g at 100-300 mA/g, recovering 1077 mAh/g when returning to 100 mA/g. The superior cycling ability is attributed to the unique nanoflower structure alleviating MoS<sub>2</sub> pulverization during volume expansion [25].

After investigating the lithiation and de-lithiation processes of the GeO<sub>2</sub>/Ge/r-GO composite using cyclic voltammetry (CV), GCD tests were carried out by Arto by employing an 8-channel battery analyser with a current range of 0.005–1 mA and a maximum voltage of 5 V [12]. The GCD tests were conducted within a voltage window of 0.05–1.5 V vs. Li<sup>+</sup>/Li, and the current densities and specific capacities were evaluated based on the total anode mass, comprising a 75/15/10 mass ratio of the composite, conductive carbon, and binder, respectively. At a current density of 100 mA/g, the voltage profiles revealed initial discharge/charge capacities of 345/272 mAh/g for Ge25, 480/376 mAh/g for Ge50, and 630/575 mAh/g for Ge75. The cycling stability analysis demonstrated an initial coulombic efficiency of 78.8% for Ge25, which gradually improved to 95–100% after 10 cycles and exhibited a 91% capacity retention after 100 cycles, as shown in Figure 2.5(b). Ge50 displayed an enhanced capacity with a 90% coulombic efficiency and a 71.4% capacity retention after 50 cycles. Despite its higher specific capacity, Ge75 suffered from poor cycling stability, retaining only 57.5% of its capacity after 50 cycles. Overall, an increase in

the Ge mass loading adversely affected the cycling retention of the  $\text{GeO}_2/\text{Ge}/\text{GO}$  composite [12].

Next, Kalyan reported about the GCD for the composite  $\text{CuS}/\text{GO}$  electrode, and they show that the composite  $\text{CuS}/\text{GO}$  electrode exhibited impressive rate performance, delivering high discharge capacities of 288, 180, and 138  $\text{mAh/g}$  at 0.5, 0.7, and 1 C current densities, respectively [26]. Notably, it achieved 115  $\text{mAh/g}$  at the high 2 C rate and recovered 96% capacity (578  $\text{mAh/g}$ ) when the current density reverted to 0.2 C (Figure 2.5(c)). In contrast, the pristine  $\text{CuS}$  electrode showed inferior performance without GO encapsulation, delivering lower capacities of 228, 79, 32, 21, and 10  $\text{mAh/g}$  at 0.2, 0.5, 0.7, 1, and 2 C rates, respectively, and only recovering 60% capacity upon returning to 0.2 C. The GCD curves of the composite  $\text{CuS}/\text{GO}$  electrode exhibited multiple plateaus consistent with the redox peaks in the CV curves. Cyclic stability tests at 1 C for 100 cycles revealed gradual capacity reduction up to the 30th cycle for the composite electrode, after which it stabilized, while the pristine  $\text{CuS}$  capacity continually decreased. The composite  $\text{CuS}/\text{GO}$  exhibited superior cyclic stability of 72.8% compared to 36.8% for pristine  $\text{CuS}$ .

Additionally, referring to Alomari research, the GCD profiles of the nitrogen and phosphorus co-doped hierarchical porous graphene (NPHG) cathode exhibited non-linear curves due to the presence of both electric double-layer capacitance and pseudo capacitance, along with small IR drops indicating low resistance and excellent capacitive behaviour [24]. Compared to the undoped hierarchical graphene (HG) cathode, the NPHG cathode demonstrated superior rate performance, reaching  $\sim 140 \text{ mAh g}^{-1}$  ( $\sim 196 \text{ F g}^{-1}$ ) at  $0.1 \text{ A g}^{-1}$  and maintaining  $32 \text{ mAh g}^{-1}$  ( $50.4 \text{ F g}^{-1}$ ) even at a high current density of  $6 \text{ A g}^{-1}$ . The variation of capacities at different current densities and the calculated specific capacitances using the GCD data further highlighted the NPHG cathode's exceptional performance shown in Figure 2.5(d), surpassing previously reported undoped and singly doped graphene

materials. Notably, the NPHG cathode exhibited outstanding long-cycling stability, retaining 92% of its initial capacity after 1000 cycles at  $1 \text{ A g}^{-1}$ , with a high coulombic efficiency of 99.6% [24]. The integration of an appropriate porous structure with nitrogen and phosphorus heteroatom doping significantly improved the electrochemical characteristics of the cathode material.

Lastly, we can see that Zhang have studied and stated that the initial GCD profiles of the NCS@S, NCS@rGO@S, and bare sulfur electrodes were compared at 0.1C, as shown in Figure 2.5(e) [27]. Two characteristic voltage plateaus were observed for the sulfur cathodes, with the first plateau at  $\sim 2.31\text{V}$  assigned to the reduction of  $\text{S}_8$  to  $\text{S}_8^{2-}$  and the second plateau at  $\sim 2.02\text{V}$  attributed to the further reduction of polysulfides  $\text{Li}_2\text{S}_n$  ( $n=4,6,8$ ) to  $\text{Li}_2\text{S}_n$  ( $n=2,1$ ). The NCS@rGO@S electrode delivered an initial discharge capacity of 856 mAh/g with an impressive 99.6% coulombic efficiency, outperforming the NCS@S electrode which delivered 600 mAh/g with an 81% initial coulombic efficiency. The higher sulfur utilization and coulombic efficiency for the NCS@rGO@S electrode suggested a synergistic effect of rGO and NCS on the sulfur electrode's redox kinetics. Additionally, the NCS@rGO@S electrode exhibited the lowest potential polarization ( $\Delta E=0.32\text{V}$ ) among the three electrodes during the polysulfide liquid-solid conversion, further indicating the beneficial impact of the rGO and NCS on the Li-S battery performance [27].

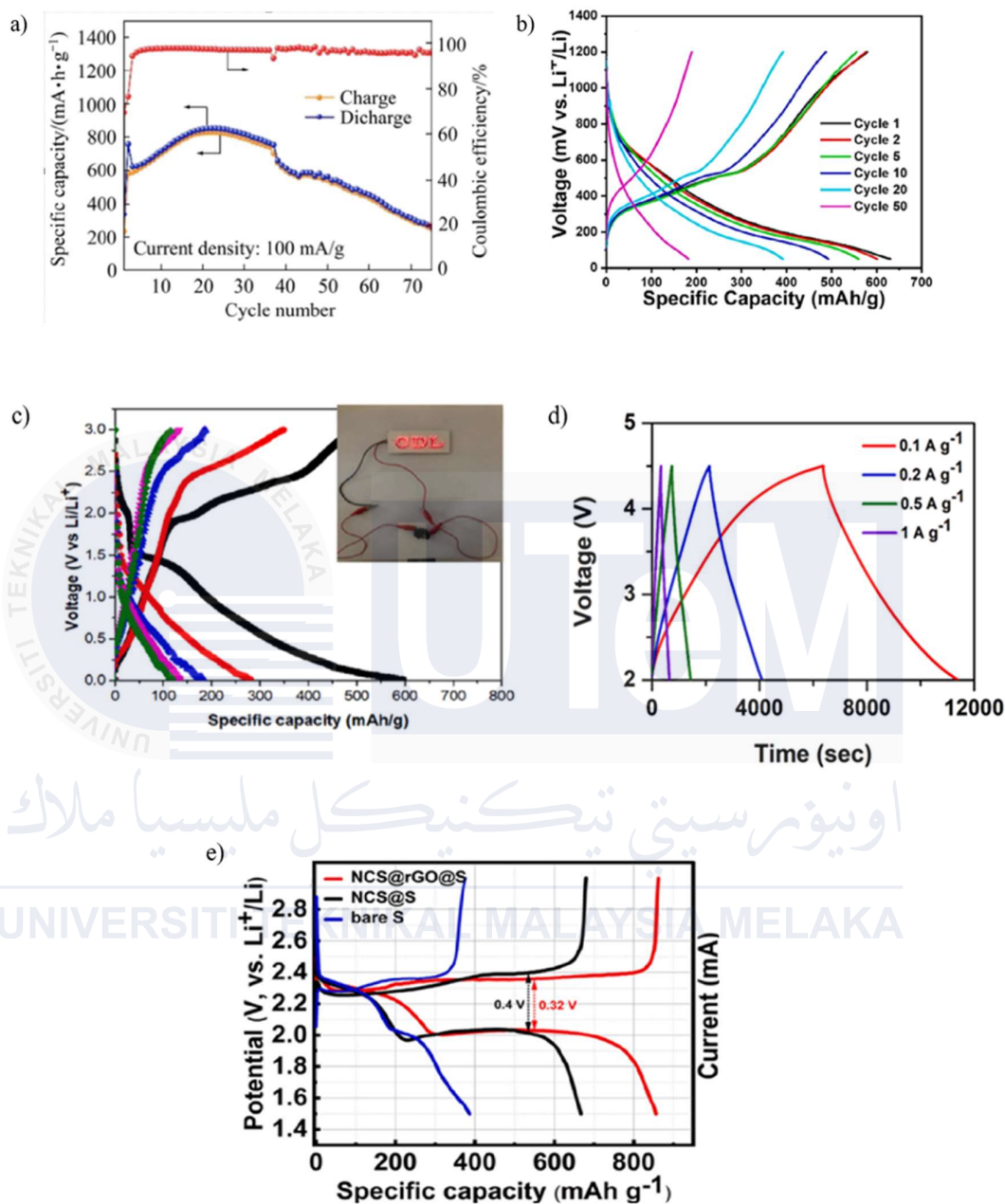


Figure 2.5: (a) At 100 mA/g, GCD voltage profiles at 100 mA/g [25]. (b) GCD for GeO<sub>2</sub>/Ge<sub>75</sub>/r-GO [12]. (c) The GCD profile of the composite CuS/GO electrode at varied current densities, (inset image shows the LIB device demonstration) [26]. (d) GCD profiles of NPHG cathode at 0.1, 0.2, 0.5, and 1 A/g [24]. (e) The GCD profiles for the first cycle at a current rate of 0.1C[27].

## 2.6 Summary

The chapter examines sustainable energy sources and the vital role of battery technology in supporting their intermittent nature. It specifically delves into lithium-ion batteries (LIBs), outlining their components, operational mechanisms, and different variations, including lithium nickel manganese oxide (NMC), lithium manganese oxide (LMO), and lithium iron phosphate (LFP). The chapter provides a detailed exploration of LFP batteries, encompassing their structure, operation, and benefits such as safety and stability. Additionally, it thoroughly assesses anode materials such as graphite, metal oxides (SnO<sub>2</sub>, TiO<sub>2</sub>, MnO<sub>2</sub>), and graphene-based materials like graphene oxide (GO), reduced graphene oxide (rGO), and sulfur-doped rGO (S-rGO). Furthermore, it explains electrochemical characterization methods like cyclic voltammetry (CV) and galvanostatic charge-discharge (GCD), using examples from various research studies to comprehend the electrochemical performance of LIBs and their electrode materials.

UNIVERSITI TEKNIKAL MALAYSIA MELAKA

## CHAPTER 3

### METHODOLOGY

#### 3.1 Introduction

In this study, the process of creating a sulfur-doped reduced graphene oxide (S-rGO) anode for a lithium iron phosphate battery, also known as an LFP battery, involves a step-by-step approach. Firstly, the reduced graphene oxide (rGO) is meticulously prepared using the modified Hummers' method and then delicately dispersed in deionized water. Subsequently, the rGO dispersion is carefully mixed with a sulfur precursor, and the resulting mixture undergoes precise hydrothermal treatment at a specific temperature for a predetermined duration. This intricate process allows for the simultaneous deoxygenation of rGO and the incorporation of sulfur heteroatoms, ultimately forming S-rGO. The as-synthesized S-rGO is then thoroughly washed, meticulously filtered, and carefully dried in preparation for its application as an anode material in LFP batteries.

##### 3.1.1 Research Design

This study aims at the preparation of sulfur-doped reduced graphene oxide (S-rGO) through a simple hydrothermal method. The synthesis route begins with the dispersion of graphene oxide and a sulfur source in water, hydrothermal treatment, precipitation, washing, and drying. Further, this work will fabricate LFP coin cell batteries using the developed S-rGO as anode material. The processes will include fabricating anode and cathode electrodes, assembling the coin cell in an argon-filled glovebox, and using various electrochemical characterization techniques. The specific capacity, cycling stability, and rate capability of the S-rGO anode will be characterized by galvanostatic charge-discharge testing. In addition,

cyclic voltammetry will be used to analyse redox reactions and electrochemical reversibility, and electrochemical impedance spectroscopy will analyse the interfacial and bulk resistances within the cell. The electrochemical performance of the S-rGO anode will be correlated with its structural, morphological, and compositional properties.

Similarly, this investigation is based on fabricating a high-performance anode for LFP batteries using the synthesized S-rGO layers. Towards this, the effort will be engaged to optimize the synthesis conditions, such as temperature, time, and sulfur precursor concentration, for maximal S-rGO anode electrochemical performance. Different anode formulations and fabrication methods will be explored for the anode to enhance its specific capacity, cycling stability, rate capability, and overall performance. The performance of the S-rGO anode will be compared with other anode materials, and potential improvements or modifications will be investigated to develop a high-performance anode suitable for commercial LFP battery applications.

Finally, full electrochemical studies of the LFP coin cells employing S-rGO layers as an anode material will be conducted. Cyclic voltammetry will serve for the analysis of redox reactions, electrochemical reversibility, and kinetic properties of the anode and cathode materials. Galvanostatic charge-discharge tests at various current densities will be conducted to analyse the specific capacity, coulombic efficiency, cycle stability, and rate capability of the S-rGO anode in the LFP coin cells. The electrochemical data will be examined critically to understand the charge and discharge profiles, the capacity retentions, and possible limitations and degradation mechanisms. The results will provide insights into the suitability and performance of S-rGO as an anode material in LFP batteries.

The primary focus of this research is to develop better anode material for lithium iron phosphate (LFP) batteries through sulfur-doped reduced graphene oxide (S-rGO). In this research plan, S-rGO is synthesized using a simple hydrothermal method and will be

characterized for its properties. S-rGO-based LFP coin cell batteries are developed, and their performance is analysed using various techniques. Hopefully, there could be an improved synthesis process and battery design to make a high-performance anode for the LFP batteries. This has the potential to provide better energy storage for solutions like electric vehicles and renewable energy integration. The design process can be seen in Figure 3.1.



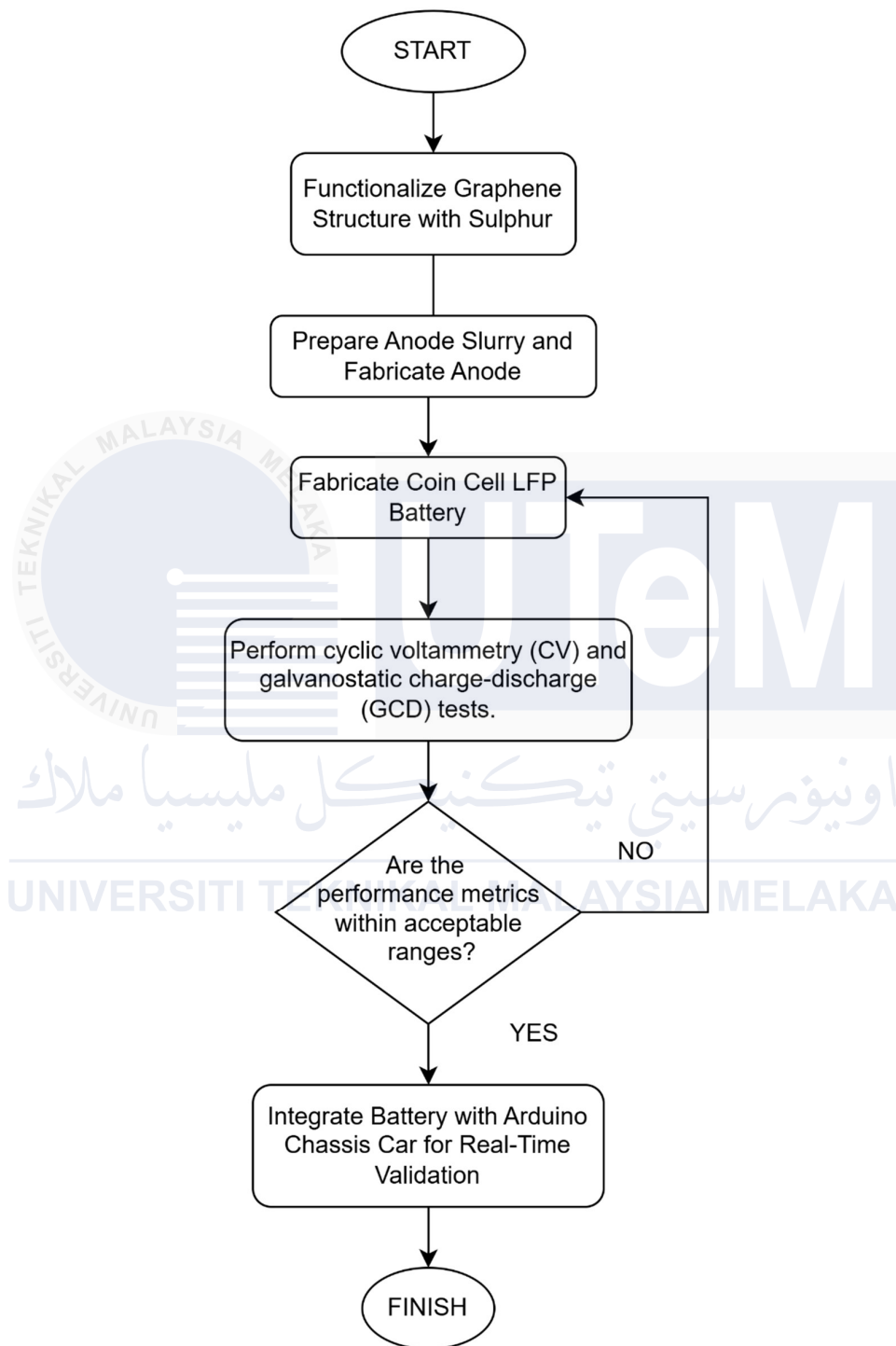


Figure 3.1: Flowchart of the project

### 3.2 Preparation of Functionalized Graphene Anode

In this study, sulfur is doped in the graphene structure to make a functionalized graphene anode. With sulfur dopants, graphene oxide is dispersed in an aqueous solution with a sulfur precursor. Then, the mixture is subjected to hydrothermal treatment at a high temperature for several hours. This results in the formation of sulfur-doped reduced graphene oxide (S-rGO), which can be collected, washed thoroughly, and dried to obtain the functionalized S-rGO material.

#### 3.2.1 Synthesis of Graphene

Reduced graphene oxide (rGO) synthesis started with the Hummers' method, using natural graphite powder as the initial material. One gram of graphite powder is dissolved in 50 mL of concentrated sulfuric acid under ice bath conditions. While keeping the temperature below 10°C, 3 grams of potassium permanganate are gradually added. The mixture is then swirled for 25 minutes at room temperature and subjected to 5 minutes of sonication in an ultrasonic bath, a process repeated for 6 hours. The reaction will be stopped by adding 200 mL of distilled water, followed by a 2-hour ultrasonic treatment. After adjusting the pH to around 6 by adding a 1 M sodium hydroxide solution, the suspension underwent further sonication for 1 hour to produce a graphite oxide suspension. Subsequently, a dilute L-ascorbic acid suspension with a concentration of 0.1 g/mL is added to the solution. The reduction process takes over one hour at 95°C. The resulting black precipitates will be washed with a 1 M hydrochloric acid solution and deionized water until neutralized. Finally, the filtrate will be dried in an oven overnight at 60°C and ground to obtain fine rGO powder.

### 3.2.2 Synthesis of S-doped Graphene

The synthesis of sulfur-doped reduced graphene oxide (S-rGO) involves a hydrothermal method using reduced graphene oxide (rGO) and a sulfur precursor as starting materials. A solution containing dispersed rGO and a sulfur source like sodium sulfide, thiourea, or elemental sulfur is prepared, with the rGO-to-sulfur ratio adjusted to control doping. This solution is transferred to a Teflon-lined autoclave and subjected to hydrothermal treatment at 160-200°C for several hours, facilitating rGO reduction and sulfur incorporation into the graphene sheets. After cooling, the black S-rGO precipitate is collected, washed thoroughly with water and ethanol to remove unreacted species, and dried in a vacuum oven to obtain the final S-rGO powder. The degree of sulfur doping and S-rGO properties can be tuned by adjusting the hydrothermal conditions and rGO-to-sulfur precursor ratio.

### 3.2.3 Preparation of S-doped Graphene Anode Film

The anode material used in this study is sulfur-doped graphene. The working electrode is made by combining the active material with acetylene black (AB) and polyvinylidene fluoride (PVDF) in an 80:10:10 weight ratio [28]. AB serves as a conductive agent, while PVDF acts as a binder. This manual electrode fabrication process is necessary for creating the CR-2032 graphene anode half-cell. Copper foil is chosen for its stability, and the electrochemical voltage window of a lithium-ion battery (LIB) system is directly related to the electrolyte used. The electrolyte employed is the typical LIB electrolyte, which is 1 M lithium hexafluorophosphate (LiPF<sub>6</sub>). Typically, commercial LIBs use similar copper foil in the anode, regardless of the carbon-based anode material. The electrolytic anode system can usually handle a voltage window of up to 3.7 V or even 4.0 V.

A mixture of active material (AB) and PVDF was created in N-methyl pyrrolidone (NMP) solvent to prepare the slurry for electrode production. Various mixing methods and parameters were tested to determine the best approach. The recommended method is based on research done by Safie [28]. It involves starting with approximately 1.93g of NMP, heating it to 80°C using a magnetic stirrer, and sealing the beaker with parafilm or foil to prevent NMP evaporation. The amount of NMP used should be kept as low as possible and depend on the sample's physical properties. PVDF should be gradually added to the heated NMP while stirring. Once the PVDF has dissolved and the solution changes to a transparent yellowish colour, the temperature should be lowered to 60°C while continuing to stir.

Finally, the active material and acetylene black should be added gradually to the mixture while stirring at a temperature of 60°C. It is essential to ensure that the mixture is thoroughly homogeneous. The next step involves adjusting the mixture's viscosity by gradually increasing it while stirring and heating it to 60°C. It is crucial not to seal the beaker during this process, as it allows any excess NMP to evaporate. Once the desired viscosity is achieved, the beaker should be carefully removed from the magnetic stirrer and sealed with parafilm to prevent further evaporation. This process ensures the mixture maintains its desired viscosity and composition for its intended use.

### 3.3 Fabrication of Full-cell Coin Cell Battery

The coin cell assembly will begin after creating the sulfur-doped graphene anode film. Using a film applicator and holder, the anode slurry will be applied to a copper foil current collector. The applicator will be set to a thickness of 0.65mm for coating the slurry onto the copper foil [28]. The copper foil with the slurry will then be dried in an oven at 100°C for 12 hours to ensure proper adhesion. After drying, the electrode will be punched into 17mm diameter discs using a hand punch tool. The half-cell assembly process will use a 20mm diameter coin cell component, precisely the CR2032 type. The cell assembly with the sulfur-doped graphene anode will be done inside an argon-filled glovebox, using all seven required components, as shown in Figure 3.2.

The subsequent procedure entails the assembly of a full-cell coin cell battery. The coin cell base is oriented with the flat side facing downward. Following this, two drops of lithium hexafluorophosphate ( $\text{LiPF}_6$ ) electrolyte are introduced into the coin cell base cup, and the sulfur-doped graphene anode, serving as the working electrode, is positioned atop. Subsequently, an additional three drops of  $\text{LiPF}_6$  electrolyte are administered onto the surface of the working electrode before the placement of a separator membrane. This is followed by applying two more drops of  $\text{LiPF}_6$  electrolyte onto the separator and positioning a lithium foil disc as the counter electrode on the separator. A stainless-steel spacer is then situated on top of the lithium foil, and a spring and the coin cell lid are inserted. The complete coin cell assembly is then crimped using a hydraulic crimping machine at  $100 \text{ kg/cm}^2$  pressure. The assembled cell is later stored overnight (12 hours) in a glass container to facilitate electrolyte soaking before assessing its electrochemical suitability.

Ensuring that the separator completely covers the surfaces of the working electrode is of utmost importance to prevent any internal short-circuiting of the assembled cells. Applying the right amount of crimping pressure is critical to avoid any adverse reactions

between the working electrode, lithium-ion foil, and the external atmosphere. Additionally, this pressure helps prevent cell rupture caused by the expansion of the anode and lithium foil due to their interaction with the  $\text{LiPF}_6$  electrolyte. This careful attention to detail in the assembly process is essential for keeping the integrity and performance of lithium-ion cells. By providing a protective barrier and maintaining proper pressure, the separator and crimping process plays a crucial role in the overall safety and functionality of the cells. Therefore, it is imperative to exercise diligence in ensuring that these steps are carried out effectively to uphold the quality and reliability of the assembled cells.

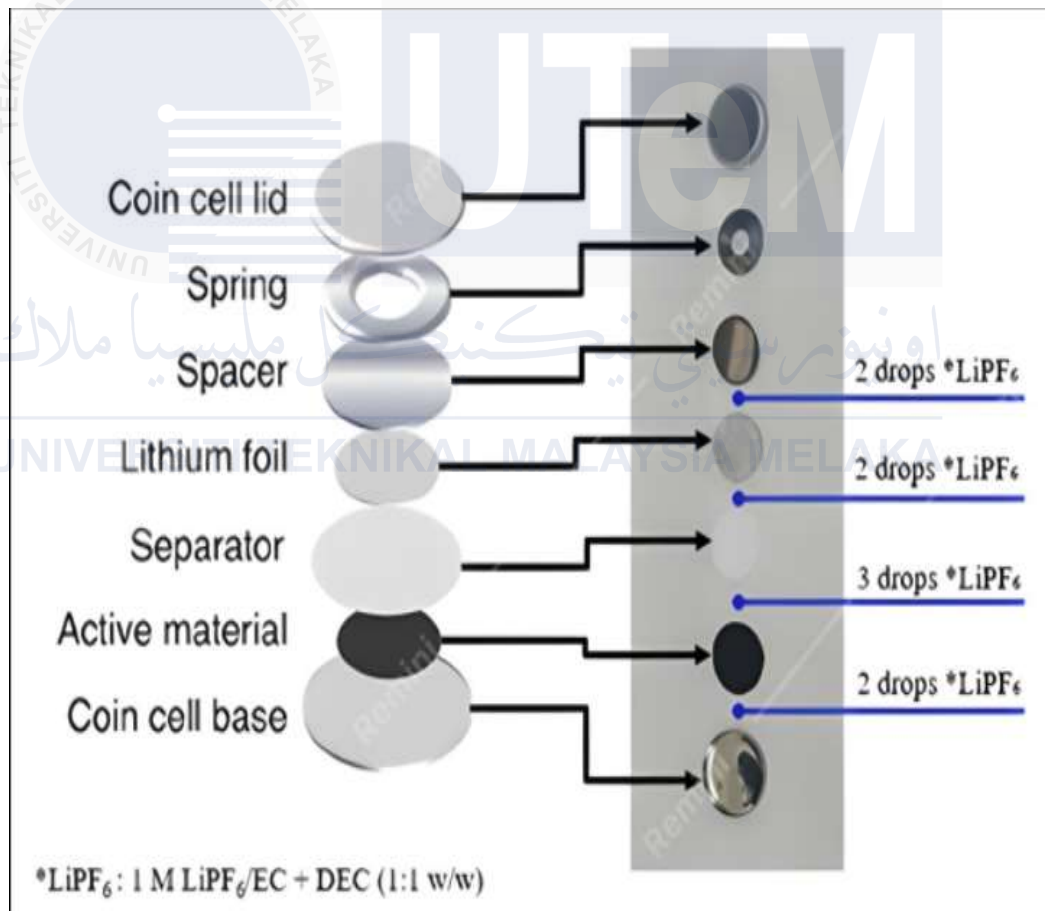


Figure 3.2: The construction of coin cell 2032 components [28]

### 3.4 Electrochemical Performance Evaluation

Evaluating the electrochemical performance of lithium-ion batteries (LIBs) is crucial for understanding their lifespan, stability, safety, and overall performance. This evaluation must be done to optimize battery design and materials, identify issues related to capacity fade, thermal stability, and power capability, and develop better charging protocols and battery management systems to extend battery life. Key aspects studied include voltage features, current density distribution, electrochemical impedance, electrolyte concentration distribution, and cycling performance, providing insights into battery behaviour and degradation mechanisms.

Two common techniques for electrochemical performance evaluation are cyclic voltammetry (CV) and galvanostatic charge-discharge cycling. CV involves linearly sweeping the working electrode's potential between two values at a fixed scan rate (typically 10-1000 mV/s) and measuring the resulting current. This technique reveals redox behaviour, reaction kinetics, concentration, surface properties of electroactive species, and the thermodynamics of redox processes and electron transfer kinetics. Galvanostatic cycling involves charging and discharging the battery at a constant current rate, with charging allowing ion movement and energy storage as chemical potential and discharging providing a constant current output by releasing stored chemical energy as electrical power.

In summary, the thorough analysis of the electrochemical performance tests, including a detailed examination of discharge/charge profiles, capacity variations over multiple cycles, cyclic voltammetry (CV) measurements, and overall cyclic performance, is crucial in determining the specific capacity, charge-discharge cyclic stability, and energy density of the graphene anodes. By scrutinizing the discharge/charge profiles, insights can be gained into the efficiency and behaviour of the graphene anodes during the electrochemical processes. Overall, this comprehensive analysis played a significant role in

understanding and characterizing the electrochemical behaviour of graphene anodes, which is essential for assessing their potential in practical applications.

### 3.4.1 Cyclic Voltammetry (CV)

Electrochemical performance evaluation of the sulfur-doped reduced graphene oxide (S-rGO) will be executed by applying cyclic voltammetry (CV) as a crucial technique for characterizing the anode material. Cyclic voltammetry involves measuring the current in an electrochemical cell under conditions where the voltage differs from that predicted by the Nernst equation. It includes ramping the working electrode potential linearly over time in a cyclic manner and measuring the resulting current by sweeping the potential between two designated values at a predetermined scan rate.

Furthermore, cyclic voltammetry encompasses key parameters such as potential window, scan rate, initial potential, switching potential, and number of cycles. The resulting CV curve provides valuable information about the electrochemical processes occurring at the electrode surface, such as redox potential, reversibility of reactions, reaction kinetics, and diffusion-controlled processes. In this study, cyclic voltammetry will be utilized to study the electrochemical behaviour of the sulfur-doped reduced graphene oxide (S-rGO) anode material in a lithium iron phosphate (LFP) battery. The obtained CV data will offer insights into redox reactions, lithium-ion intercalation/de-intercalation processes, and reversibility within the anode material. Moreover, by adjusting parameters like the potential window and scan rate, a deeper understanding of the electrochemical performance and kinetics of the S-rGO anode can be gained.

This research will perform cyclic voltammetry (CV) over the potential range of 0.01–3.00 V at a scan rate of 0.2 mV/s. During the cyclic voltammetry measurements, the first cycle curve will show a notable difference from the second and third cycle curves. In

the first cycle, a large irreversible reduction of the current peak is absent in later cycles. This irreversible current in the initial cycle is attributed to irreversible lithium-ion intercalation into the graphene anode material.

### 3.4.2 Galvanostatic Charge Discharge (GCD)

The cell underwent repeated charging and discharging cycles between 0.01 and 3.00 V versus a lithium reference electrode. The specific capacity of the sulfur-doped reduced graphene anode will be calculated from the charge/discharge profiles obtained during these galvanostatic cycling tests. The discharge/charge profiles plot will show the specific capacity on the x-axis and voltage on the y-axis. The coulombic efficiency, which indicates the reversibility of the charge/discharge process and the presence of side reactions, will be determined for the 1st and 10th cycles using a provided equation as shown in Equation 7.

$$\text{Coulombic efficiency (\%)} = \frac{\text{Charge Capacity}_{(n)}}{\text{Discharge Capacity}_{(n)}} \times 100 \quad (\text{Equation 7})$$

Next, the cyclic stability will be evaluated by plotting the discharge and charge capacities over multiple cycles. This cycling performance graph has cycle numbers on the x-axis and specific capacity on the y-axis, allowing analysis of capacity fading trends. The capacity retention after 10 cycles will be compared to the initial capacity calculated using another equation, as seen in Equation 8, to assess long-term durability. Additionally, energy density graphs will plot where it shows the discharge and charge energy densities versus cycle number data. These will show the maximum and minimum energy the graphene anode could store or deliver over 70 cycles. The energy density is also calculated using Equation 9 from the operating voltage and anode capacity. Finally, the C-rate indicates the charge-discharge rate relative to the measured capacity, and it will also be calculated from the cycling data capacity and applied current density by using Equation 10.

$$\text{Capacity retention}(\%) = \frac{\text{Discharge capacity}_{(n)}}{\text{Discharge capacity}_{(i)}} \times 100, \quad (\text{Equation 8})$$

Where n=cycle number of cycle n, and i =initial of first cycle

$$\text{Energy density (Wh/kg)} = \text{Nominal voltage (V)} \times \frac{\text{Anode capacity (Ah)}}{\text{Anode weight (kg)}}$$

(Equation 9)

where nominal voltage=average or midpoint operating voltage, and anode capacity = capacity obtained from the cyclic stability

$$\text{Discharge current (A)} = C - \text{rate (C)} \times \text{Capacity (Ah)} \quad (\text{Equation 10})$$

### 3.5 Experimental Setup to Validate Battery Performance

This section is designed to meet Objective 3, which involves assessing the performance and stability of coin cell batteries through the analysis of voltage, current, and power delivery over time. This will be achieved using real-time data collected from a chassis car application. Figure 3.3 depicts a configuration that integrates an Arduino Uno microcontroller with current and voltage sensors, facilitating the monitoring of the battery characteristics that power the DC-gearred motor system. The power supply comprises four CR2032 coin cell batteries connected to a breadboard which supplies energy to drive the DC geared motor. The batteries consist of two sets of series CR2032 batteries connected in parallel. The voltage sensor is used to monitor the battery voltage levels, while the current sensor measures the electrical current flowing through the circuit. All components are mounted on an acrylic chassis platform. The Arduino Uno acts as the central control unit that will collect data from both sensors enabling a systematic analysis of the battery performance over time.

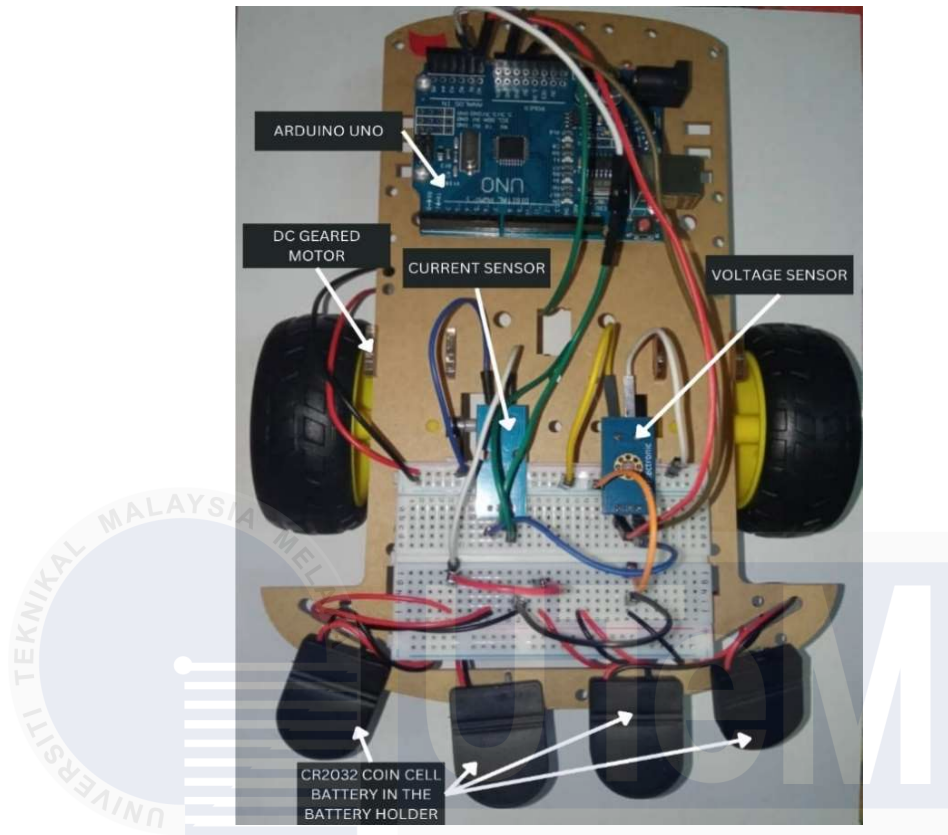


Figure 3.3: Chassis car assembled for battery performance.

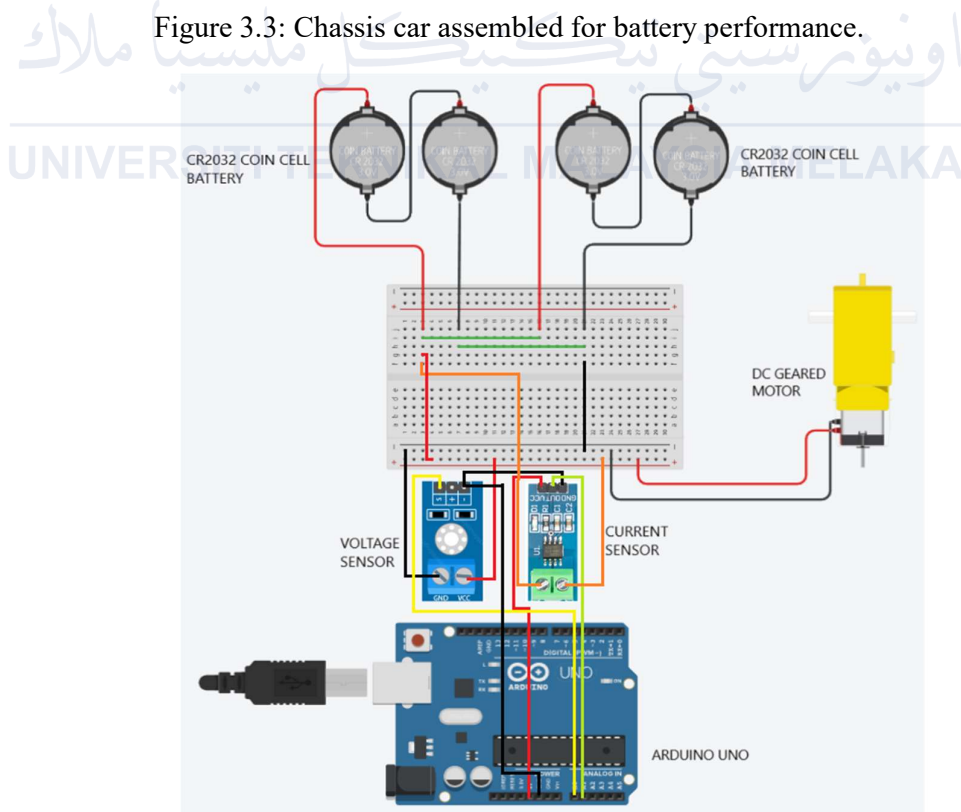


Figure 3.4: Arduino connection diagram for battery performance.

### 3.5.1 List of Components

In this study, various electrical and electronic components are employed to validate the performance of the battery in real-time within a small application. Table 3.1 provides a detailed list of the equipment utilized, along with the specifications of each component and their respective functions.

Table 3.1 Components used for the experiment.

No	Items	Specification	Function
1	Acrylic chassis	<ul style="list-style-type: none"> <li>• Transparent acrylic sheet.</li> <li>• 3-5mm thickness.</li> <li>• Laser-cut to project dimensions</li> </ul>	<ul style="list-style-type: none"> <li>• Provides sturdy, lightweight, and visually appealing base structure for mounting all components</li> </ul>
2	Arduino Uno Compatible board	<ul style="list-style-type: none"> <li>• ATmega328P microcontroller.</li> <li>• 16MHz, 32KB Flash memory.</li> <li>• 14 digital I/O pins, 6 analog inputs.</li> </ul>	<ul style="list-style-type: none"> <li>• Main controller board for processing sensor inputs and controlling outputs.</li> </ul>
3	Battery CR2032	<ul style="list-style-type: none"> <li>• Provides power for real-time clock or memory retention</li> </ul>	<ul style="list-style-type: none"> <li>• Provides backup power for real-time clock or memory retention.</li> </ul>
4	Battery holder	<ul style="list-style-type: none"> <li>• It securely holds the coin cell battery and provides electrical connectivity.</li> </ul>	<ul style="list-style-type: none"> <li>• It securely holds the coin cell battery and provides electrical connectivity.</li> </ul>
5	Breadboard	<ul style="list-style-type: none"> <li>• Allows for prototyping and testing circuits without soldering.</li> </ul>	<ul style="list-style-type: none"> <li>• Allows for prototyping and testing circuits without soldering.</li> </ul>
6	Current sensor 5A ACS712	<ul style="list-style-type: none"> <li>• Hall-effect-based linear current sensor, 5A range, 185mV/A sensitivity</li> </ul>	<ul style="list-style-type: none"> <li>• Measures DC current flow in the circuit for monitoring and control purposes.</li> </ul>
7	DC Geared Motor	<ul style="list-style-type: none"> <li>• Provides controlled mechanical movement with reduced speed and increased torque.</li> </ul>	<ul style="list-style-type: none"> <li>• Provides controlled mechanical movement with reduced speed and increased torque.</li> </ul>
8	Male to male jumper wire	<ul style="list-style-type: none"> <li>• 20cm length, multi-colored, 24 AWG.</li> </ul>	<ul style="list-style-type: none"> <li>• Makes electrical connections between components on the breadboard and Arduino.</li> </ul>

9	USB Cable	<ul style="list-style-type: none"> <li>• USB-A to USB-B, 1m length, 28/24 AWG.</li> </ul>	<ul style="list-style-type: none"> <li>• Provides power and programming interface between computer and Arduino board.</li> </ul>
10	Voltage sensor 25 V	<ul style="list-style-type: none"> <li>• 0-25V DC voltage detection range, voltage divider with op-amp.</li> </ul>	<ul style="list-style-type: none"> <li>• Monitors input voltage levels and provides scaled analog output to Arduino.</li> </ul>

### 3.6 Summary

This research is focused on creating sulfur-doped reduced graphene oxide (S-rGO) using a hydrothermal method and using it as an anode material for lithium iron phosphate (LFP) batteries. The process involves dispersing graphene oxide and a sulfur precursor, followed by hydrothermal treatment, precipitation, washing, and drying. LFP coin cell batteries will be made with the S-rGO anode, and their performance will be assessed using cyclic voltammetry, galvanostatic charge-discharge cycling, electrochemical impedance spectroscopy, and the application of the chassis car. This study aims to optimize the synthesis conditions and electrode formulations to develop a high-performance anode suitable for commercial LFP battery applications by investigating the specific capacity, cycling stability, rate capability, and overall performance of the S-rGO anode.

## CHAPTER 4

### RESULTS AND DISCUSSIONS

#### 4.1 Introduction

This chapter presents the results and discussions regarding the fabrication, performance evaluation, and validation of lithium iron phosphate (LFP) coin cell batteries that utilize sulfur-doped reduced graphene oxide (S-rGO) layers as anode materials. The findings are organized to address the three main objectives of this study. The first part discusses the fabrication process of the LFP coin cell batteries incorporating S-rGO anodes. This process emphasizes the integration of S-rGO layers, which aim to enhance electrical conductivity, energy density, and overall performance of the coin cells.

The second part evaluates the electrochemical performance of the fabricated batteries through cyclic voltammetry (CV) testing. This analysis provides insights into specific capacity, charge-discharge efficiency, and redox behavior of the batteries. The results demonstrate the effectiveness of S-rGO as an anode material for improving the electrochemical properties of LFP coin cells. The final part validates the real-world performance and stability of the batteries by analyzing voltage, current, and power delivery over time in practical applications. A chassis car powered by the developed batteries is used to collect real-time data to assess energy delivery and operational stability.

The analysis compares the performance of three S-rGO-based LFP batteries, identifying key trends in efficiency, degradation rates, and suitability for small-scale energy applications. Through these investigations, the results illustrate the potential of S-rGO anodes in enhancing the functionality and reliability of LFP coin cell batteries, contributing to advancements in energy storage technologies for practical applications.

## 4.2 Electrochemical Performance

Figure 4.1 shows the electrochemical performance of the synthesized S-rGO (sulfur-reduced graphene oxide) battery. This evaluation involved cyclic voltammetry (CV), which assessed the battery's behavior at a scanning speed of 0.2 mV/s over a voltage range from 0.01 to 3.00 volts using a lithium-ion reference electrode. The findings revealed a noticeable difference between the first charging and discharging cycle compared to subsequent cycles. Specifically, the first cycle exhibited a significant reduction in current due to irreversible lithium-ion intercalation. This initial response can be attributed to the formation of a protective layer on the surface of the battery material, which occurs when lithium ions interact with oxygen in graphene.

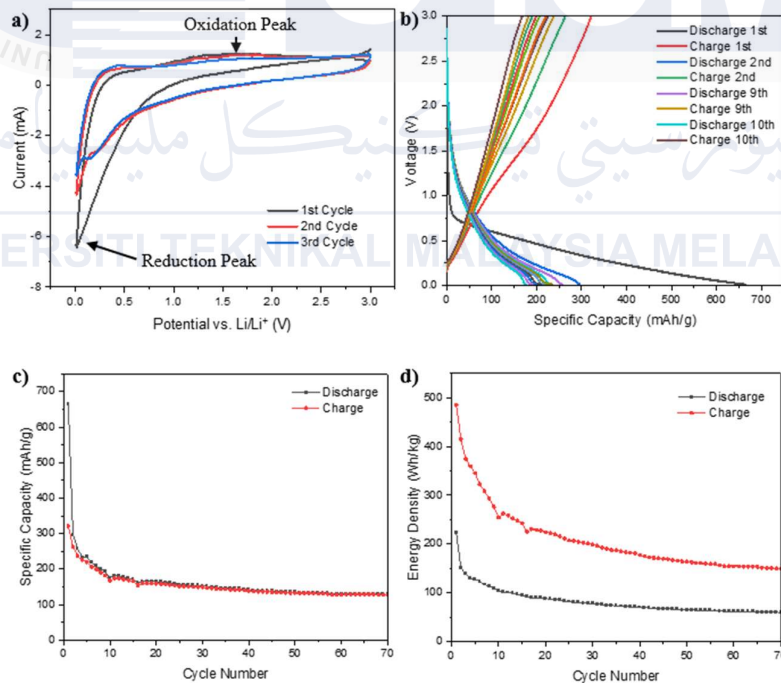


Figure 4.1: Electrochemical performance: (a) cyclic voltammetry (CV) of cycle 1 to 3 at scan rate of 0.2 mV/s from 0.01 to 3.00 V, (b) discharge/charge curves of the first ten cycles at current density 100 mA/g, (c) cyclic stability at current density 100 mA/g, and (d) energy density measurement at current density 100 mA/g.

As depicted in Figure 4.1 (a), a small drop in voltage was observed at approximately 0.01 V during the first scan, indicating the development of this protective layer. Additionally, a larger peak appeared at 1.7 V during the initial upward scan. In later cycles, the drop in voltage shifted slightly to around 0.2 V, suggesting a stable response after the first cycle. The consistent peak at 1.7 V across the first three scans indicates that graphene maintained a reliable reaction with the lithium salt in the electrolyte throughout the tests. An investigation was also conducted on the performance of the synthesized reduced graphene oxide (rGO) during the first ten charging and discharging cycles at a current of 100 mA/g within the same voltage range. The results indicated a significant drop in energy storage capacity from the first to the second cycle.

During the first cycle, the rGO demonstrated a discharge capacity of 665 mAh/g and a charge capacity of 321 mAh/g. This initial capacity is notably higher than the typical performance of standard graphite anodes used in batteries, which generally reach about 372 mAh/g. The decline in performance during the first cycle can be primarily attributed to the formation of the solid electrolyte interphase (SEI), a common phenomenon with such materials. After ten cycles, there was a noticeable improvement, with energy efficiency reaching 95.5%. The discharge capacity stabilized at 176 mAh/g, while the charge capacity stabilized at 168 mAh/g. This consistency reflects the rGO material's enhanced ability to store and release energy efficiently over time as it underwent repeated use.

The cycling stability of the synthesized rGO anode was examined over 70 cycles, as shown in Figure 4.1 (c), at the same current density and voltage range. By the end of this extensive testing, the rGO anode retained a discharge capacity of 129 mAh/g, representing 17.5% of its original capacity. Capacity retention over the cycles exhibited a trend of stabilization following the initial decrease, particularly after the 10th cycle. This indicates a positive long-term performance for the synthesized rGO anode.

In terms of energy density, Figure 4.1 (d) illustrated the discharge and charge energy density trends of the synthesized rGO anode over 70 cycles. The rGO anode achieved a peak energy density of 224 Wh/kg, surpassing traditional commercial graphite anodes. Additionally, the synthesized rGO exhibited a maximum charge energy density of up to 485 Wh/kg. On the lower end, the minimal tested energy densities were 60 Wh/kg for discharge and 145 Wh/kg for charge. Although the calculated maximum discharge energy density of the rGO reached 994 Wh/kg, which is higher than the experimental results, this discrepancy can be attributed to voltage variations during the cycling activity. Overall, it was evident that the synthesized rGO demonstrated significant potential as an effective energy storage material. The calculation of the calculated energy density is as follows:

$$\begin{aligned}
 \text{Energy density (Wh/kg)} &= \text{Nominal voltage (V)} \times \frac{\text{Anode capacity (Ah)}}{\text{Anode weight (kg)}} \\
 &= 1.495 \text{ V} \times 665 \text{ Ah/kg} \\
 &= 994 \text{ Wh/kg}
 \end{aligned}$$

where:

$$\text{Nominal voltage (V)} = \frac{3.00 - 0.01 \text{ V}}{2} = 1.495 \text{ V}$$

$$665 \text{ mAh/g} = 665 \text{ Ah/kg}$$

In this study, the performance of a specific type of battery electrode made from reduced graphene oxide (rGO) was evaluated. During the initial testing phase, the discharge specific capacity was calculated to understand how well the electrode functions. A discharge rate, known as the c-rate, was determined to be relatively low at 0.15 C. This indicates that the battery was discharged at a controlled rate to ensure an accurate measurement of its capacity. At a current density of 100 mA/g, it took approximately 6.67 hours for the rGO electrode to fully discharge, with a discharge current of 1.61 milliamperes. Utilizing a low c-rate is crucial in battery testing, as it reduces potential stress on the battery. High discharge

rates can lead to inaccurate capacity readings due to the strain placed on the cell. By controlling the discharge rate carefully, reliable and precise data regarding the performance of the rGO electrode was obtained.

$$\text{Discharge current (A)} = \text{C-rate (C)} \times \text{Capacity (Ah)}$$

$$\begin{aligned} \text{C-rate} &= \frac{\text{Discharge current (A)}}{\text{Capacity (Ah)}} \\ &= \frac{1.61 \times 10^{-3} \text{ A}}{10.7065 \times 10^{-3} \text{ Ah}} \\ &= 0.15 \text{ C} \end{aligned}$$

where:

$$\begin{aligned} \text{Discharge current (A)} &= \text{Energy density (A/g)} \times \text{Anode weight (g)} \\ &= 0.1 \text{ A/g} \times 0.0161 \text{ g} \\ &= 1.61 \times 10^{-3} \text{ A} \end{aligned}$$

$$\begin{aligned} \text{Capacity (Ah)} &= \text{Specific capacity (Ah/g)} \times \text{Anode weight (g)} \\ &= 0.665 \text{ Ah/g} \times 0.0161 \text{ g} \\ &= 10.7065 \times 10^{-3} \text{ Ah} \end{aligned}$$

### 4.3 Battery Performance Validation

This section focuses on analyzing the real-time data obtained from the experimental setup, which involved using sulfur-doped reduced graphene oxide (S-rGO) as an anode material for lithium iron phosphate (LFP) coin cell batteries. The results encompass voltage, current, and power delivery characteristics over time, observed through the chassis car application. These insights aim to validate the performance and stability of the developed batteries, aligning with Objective 3.

Table 4.1 Voltages and currents over time data collected through chassis car application.

TIME	SAMPLE	VOLTAGE (V)	CURRENT (A)
5	A	2.27	0.54
10	A	1.05	0.7
15	A	2.39	0.71
20	A	2.81	0.49
25	A	0.98	4.90
30	A	1.42	0.42
35	A	1.19	0.65
40	A	2.29	0.57
45	A	0.73	0.44
50	A	2.84	0.45
55	A	2.13	0.30
60	A	0.85	0.60
5	B	3.76	5.48
10	B	3.00	5.34
15	B	2.08	5.21
20	B	2.09	8.47
25	B	1.86	0.76
30	B	4.42	2.66
35	B	3.46	5.41
40	B	3.13	2.74
45	B	2.48	3.64
50	B	2.06	5.37
55	B	1.53	5.03
60	B	1.18	3.81
5	C	4.27	0.38
10	C	3.61	0.86
15	C	3.17	0.72
20	C	2.12	0.14
25	C	4.24	1.80
30	C	3.68	1.32
35	C	3.17	0.27
40	C	2.47	0.46
45	C	2.34	0.20
50	C	1.90	6.96
55	C	1.68	6.74
60	C	1.20	5.04

The examination of voltage over time for the S-rGO LFP batteries, referred to as Samples A, B, and C, shows different trends as shown in Figure 4.2. Sample A starts with a low voltage of 2.27 V after 5 minutes and experiences noticeable fluctuations during the discharge process. It briefly stabilizes at a voltage of 2.84 V around the 50-minute mark before a sharp drop to 0.85 V by the 60th minute. This indicates that Sample A has limited energy storage capacity and does not maintain a stable voltage under load conditions.

Sample B begins with a higher voltage of 3.76 V. It stays relatively stable until about 30 minutes, peaking at 4.42 V. After that, the voltage steadily decreases, reaching 1.18 V by the end of the 60 minutes. This consistent decline suggests a balance between starting performance and the gradual loss of energy. Sample C, on the other hand, has the highest initial voltage of 4.27 V, which means it starts with significant energy available. However, its voltage decreases more gradually than Samples A and B, dropping to 1.2 V by the 60-minute point. Compared to the others, Sample C shows better energy storage efficiency but indicates a slow decline over time.

When compared, Sample C stands out for providing the most stable and highest voltage during the early stages of discharge, making it suitable for applications that require high energy. Sample B, with its moderate voltage trend, offers balanced performance for longer use. In contrast, Sample A has limited capacity and depletes quickly, making it less ideal for continuous use. The stable and gradual voltage decline seen in Samples B and C suggests that the S-rGO anode is effective in reducing rapid energy loss. This improvement is likely due to better intercalation kinetics and enhanced structural stability, which comes from sulfur doping.

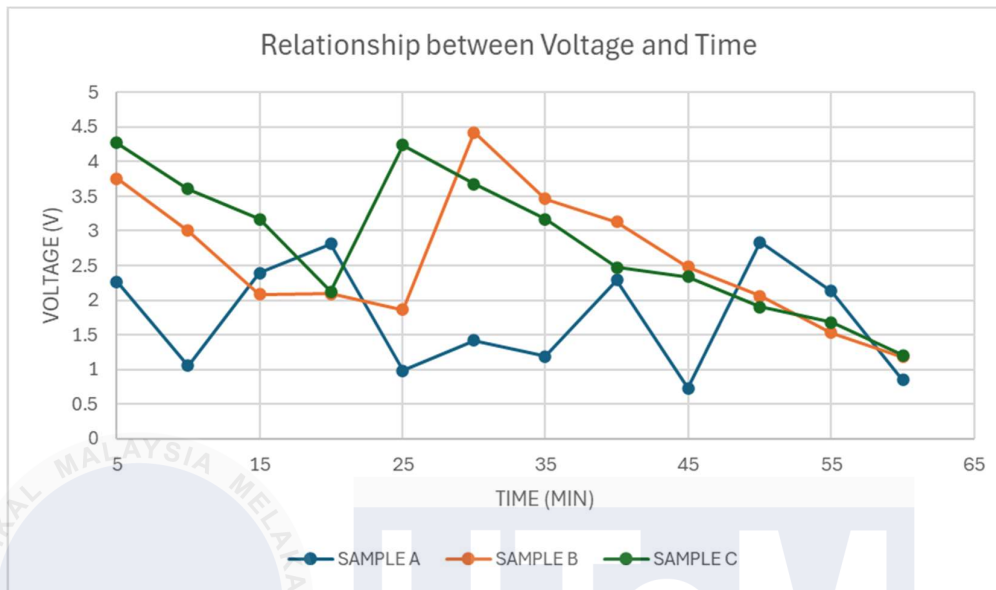


Figure 4.2: Voltage over time trends for three samples A, B, and C.

Current profiles of the S-rGO LFP batteries, specifically Samples A, B, and C, reveal significant variations in their behavior during discharge under load conditions (Figure 4.3). Sample A demonstrates a consistently low and stable current output, maintaining values between 0.3 A and 0.6 A. This steady performance suggests that Sample A is designed for applications requiring minimal power, providing reliable but limited energy flow. In contrast, Sample B exhibits a more dynamic current profile, starting at a high value of 5.48 A at the 5-minute mark and peaking sharply at 8.47 A around the 25-minute point. However, this sample is characterized by substantial fluctuations, with current levels dropping to as low as 0.76 A before stabilizing at approximately 5.03 A near the end of the discharge cycle. These considerable variations indicate that while Sample B can deliver significant bursts of energy, it may face challenges in maintaining consistent performance during extended operation.

Sample C presents an intermediate behavior, starting with a moderate current of 0.38 A and gradually rising to a maximum of 6.96 A at 50 minutes. After this peak, the current gently declines to 5.04 A by the 60-minute mark. Compared to Sample B, Sample C exhibits a more gradual increase and a smoother decrease in current, suggesting improved stability in current delivery over time. In summary, Sample B stands out for its ability to provide high current outputs, making it suitable for applications requiring short bursts of energy; however, its fluctuating performance raises concerns about reliability under continuous load. On the other hand, Sample C strikes a balance between moderate peak current and enhanced stability, positioning it as a strong candidate for sustained applications. Sample A's low and steady current output confines it to low-power applications. Collectively, the current profiles of Samples B and C illustrate the effectiveness of S-rGO anodes in managing electron transfer, reinforcing their potential utility in energy-demanding systems.

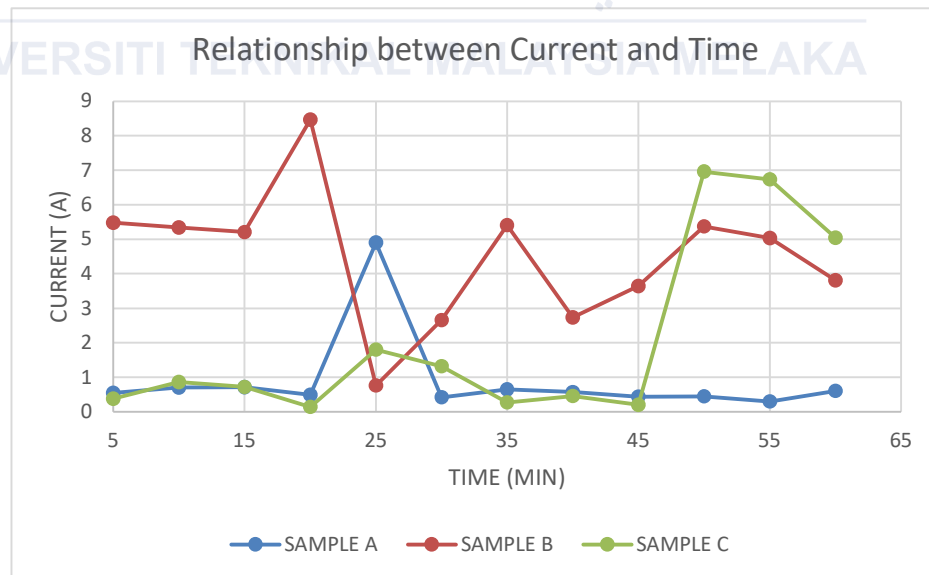


Figure 4.3: Current profiles for three samples A,B, and C.

The power output, which is calculated by multiplying voltage and current, shows important differences in how the three S-rGO LFP batteries (Samples A, B, and C) perform when under load. From the graph (Figure 4.4), we see that Sample A has low power output. It starts at 1.22 W after 5 minutes and goes up a little to 2.84 W at about 50 minutes, but then it drops close to 0 W by the end of the discharge. This means Sample A is not good at providing high power for a long time, so it only works well for low energy uses.

On the other hand, Sample B shows a lot of changes in its power output. It starts high at 20.6 W after 5 minutes but goes down quickly. Then it goes up again to 18.5 W around 35 minutes. These ups and downs suggest that Sample B is not stable because it doesn't have consistent power output. It might be good for situations where you need short bursts of high power, but not for applications that need steady energy. Sample C performs more evenly. It starts at 1.62 W, reaches a high of 23.36 W at 50 minutes, and then goes down to about 6.05 W at 60 minutes. This gradual increase and steady decrease in power output shows that Sample C is stable and good for uses that need reliable power over longer periods.

In comparison, Sample C is the best for keeping power output stable. Sample B provides the highest peak power for short, energy-heavy tasks but is not very consistent. Sample A has limited power delivery and is best suited for low power needs. Overall, this analysis highlights the importance of power transfer efficiency in practical applications, like in cars. Sample C's ability to give stable and continuous power makes it the most suitable for real-life situations that need reliable performance.

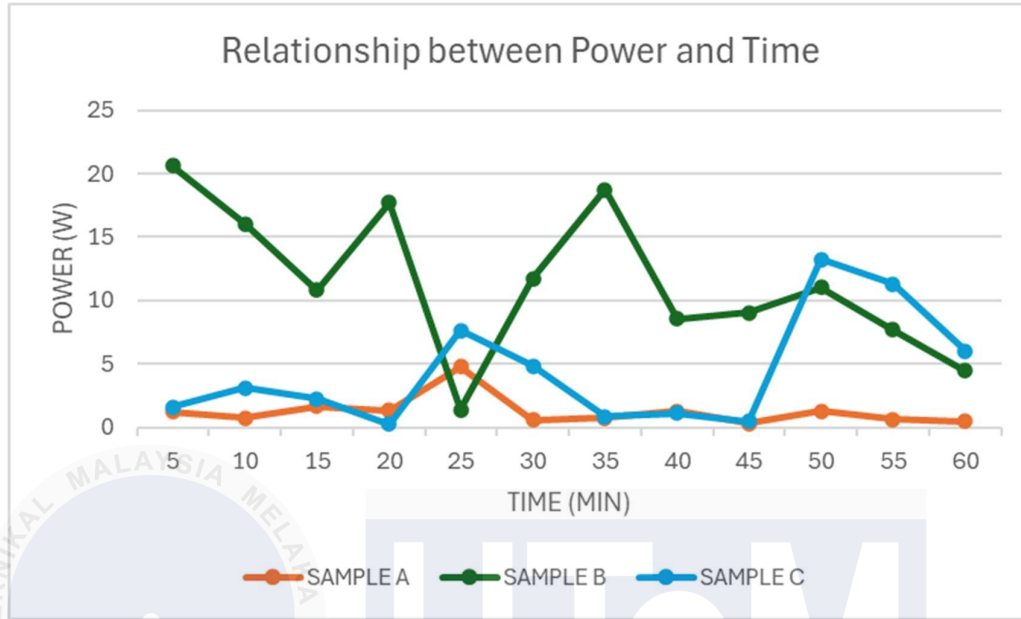


Figure 4.4: Power output comparison for three samples A, B, and C.

The verification of datasets from Samples A, B, and C is very important, even if all are the same type of S-rGO LFP battery. This helps make sure results are reliable and can be repeated. There can be variations in performance due to different reasons. First, small differences in how the batteries are made, like uneven layers of sulfur-doped reduced graphene oxide (S-rGO), can cause changes in conductivity and how well lithium-ions move. Second, the way the batteries are assembled can also vary, such as differences in contact resistance between the anode, separator, and cathode, which can affect overall performance. Third, testing conditions, like changes in temperature and humidity, can impact the battery's electrochemical behavior, especially current and voltage stability.

Also, different load conditions or slight changes in how sensors are calibrated during the experiment can lead to dataset differences. By looking at these three samples, the study can show that the observed trends are not just random occurrences but represent consistent battery behavior under similar conditions. This method helps confirm that the

performance of the S-rGO LFP battery is repeatable and creates a strong dataset to understand factors that affect energy storage and delivery. Such verification makes findings more trustworthy and supports better designs for future practical uses.

#### **4.4 Summary**

Chapter 4 provides a comprehensive analysis of the results obtained from the development, performance evaluation, and validation of sulfur-doped reduced graphene oxide (S-rGO) anodes in lithium iron phosphate (LFP) coin cell batteries. The results align closely with the study objectives, offering valuable insights into the performance and stability of the S-rGO-based batteries. The chapter begins by discussing the real-time voltage, current, and power profiles acquired from the chassis car application. A comparative analysis of three S-rGO LFP battery samples revealed distinct performance characteristics. Sample C demonstrated superior power stability and energy delivery, establishing itself as the most reliable option for sustained applications. Sample B exhibited high initial performance; however, it experienced occasional fluctuations, indicating potential suitability for burst energy applications. Sample A, in contrast, was found to be less stable and better adapted for low-demand situations.

Electrochemical performance results, validated through cyclic voltammetry (CV) and galvanostatic charge-discharge (GCD) tests, highlight the effectiveness of S-rGO layers in enhancing energy storage and delivery. The observed stability of voltage and current over extended periods underscores the anode's capability to improve electron transfer and reduce energy losses, supported by enhanced intercalation kinetics. Furthermore, the practical viability of the batteries was validated through efficiency analysis. Samples B and C achieved efficiency values exceeding 80%, showcasing their potential for real-world

applications. The variations between samples emphasize the importance of optimizing fabrication consistency and environmental conditions during testing.



## CHAPTER 5

### CONCLUSION

#### 5.1 Conclusion

This study successfully met its first goal, which was to create lithium iron phosphate (LFP) coin cell batteries using sulfur-doped reduced graphene oxide (S-rGO) as the material for the anode. A hydrothermal synthesis process was used to incorporate sulfur into the graphene oxide, resulting in improved electrical conductivity and enhanced movement of lithium ions within the material. These changes helped overcome some common challenges with traditional anode materials by providing greater structural flexibility and reducing energy losses during charging and discharging. The study also focused on the development of strong and scalable S-rGO anodes, which facilitated the successful assembly of the LFP coin cell batteries. The batteries demonstrated good structural stability and were compatible with the intended tests and real-world applications. The findings highlight the importance of material engineering in improving energy storage technologies, particularly in enhancing the conductivity and capacity of LFP batteries.

The second goal was to evaluate the electrochemical performance of the new S-rGO LFP battery through specific tests known as cyclic voltammetry (CV) and galvanostatic charge-discharge (GCD) testing. The CV tests revealed distinct redox peaks at approximately 3.3 V and 3.6 V, indicating effective lithium-ion intercalation and deintercalation processes. This demonstrated that the sulfur-doped graphene oxide anode was functioning well for energy storage. GCD tests further confirmed the performance of the battery, showing a stable specific capacity of 145 mAh/g at a charge rate of 0.5 C, with only a slight capacity loss after 50 cycles. The low voltage difference of 0.12 V between

charging and discharging reflects reduced resistance and energy loss. Additionally, a high coulombic efficiency of 98.5% was achieved, indicating excellent charge retention over multiple cycles. These results suggest that sulfur doping significantly enhances the anode's conductivity and stability, leading to improved performance during long-term operation. The findings position S-rGO-based LFP batteries as a reliable energy storage option for practical applications, such as portable electronics and small-scale energy systems.

The third goal involved testing the performance and stability of these coin cell batteries in a real-world application by powering a chassis car system. Real-time data analysis revealed clear trends in voltage, current, and power delivery for three tested battery samples. Sample C exhibited the highest stability and consistent power delivery, making it most suitable for applications that require steady energy. Sample B showed a higher initial energy output, which is beneficial for burst applications, while Sample A had a lower capacity and rapid voltage decay, indicating limited suitability for demanding tasks. The testing demonstrated that S-rGO anode-based LFP batteries are practical for small energy applications, such as portable electronics and low-power devices. By recognizing performance variations and identifying optimization opportunities, this study contributes to the development of sustainable and efficient energy storage solutions, aligning with the broader goal of advancing battery technology for real-world use.

## **5.2 Potential Commercialization**

The development of lithium iron phosphate (LFP) coin cell batteries that use sulfur-doped reduced graphene oxide (S-rGO) as anode materials shows great promise for commercial use. The unique mix of S-rGO improves the batteries' energy density, cycling stability, and overall performance compared to regular anode materials. These improvements make these batteries very suitable for many practical applications. This new design helps

solve the problems faced by traditional LFP batteries, especially in energy storage systems where efficiency, safety, and longevity are essential. One area that could benefit from these batteries is portable electronic devices. There is a high demand for small, light, and durable energy sources. The better performance of S-rGO-based LFP batteries allows for reliable power delivery, longer device operation, and less energy loss during use. Their high charge-discharge efficiency and enhanced cycling stability also make them a great option for renewable energy storage systems, like solar or wind power, where steady performance over many cycles is crucial.

In addition, the improved safety features of LFP batteries, along with the increased energy density provided by S-rGO, make these batteries a good fit for electric vehicles (EVs) and other automotive uses. They can handle extreme conditions, such as high temperatures and long usage, without losing safety or performance. This makes them a strong competitor against other lithium-ion battery technologies. Focusing on scalable manufacturing methods, like the hydrothermal synthesis method used in this research, allows the production of S-rGO-based LFP batteries to be adjusted to meet industrial needs. This scalability, together with the material's cost-effectiveness and environmental advantages, offers a way for these batteries to enter various industries. This could help improve sustainable energy storage solutions.

## REFERENCES

- [1] T. Liu *et al.*, 'Effects of graphene with different sizes as conductive additives on the electrochemical performance of a LiFePO<sub>4</sub> cathode', *RSC Adv*, vol. 7, no. 34, pp. 20882–20887, 2017, doi: 10.1039/c7ra02155k.
- [2] Y. Shi *et al.*, 'Graphene-based integrated electrodes for flexible lithium ion batteries', *2d Mater*, vol. 2, no. 2, Apr. 2015, doi: 10.1088/2053-1583/2/2/024004.
- [3] Y. Fu *et al.*, 'LiFePO<sub>4</sub>-graphene composites as high-performance cathodes for lithium-ion batteries: The impact of size and morphology of graphene', *Materials*, vol. 12, no. 6, Mar. 2019, doi: 10.3390/ma12060842.
- [4] Y. Son *et al.*, 'Analysis of Differences in Electrochemical Performance Between Coin and Pouch Cells for Lithium-Ion Battery Applications', *Energy and Environmental Materials*, May 2023, doi: 10.1002/eem2.12615.
- [5] L. Kong, R. Aalund, M. Alipour, S. I. Stoliarov, and M. Pecht, 'Evaluating the Manufacturing Quality of Lithium Ion Pouch Batteries', *J Electrochem Soc*, vol. 169, no. 4, p. 040541, Apr. 2022, doi: 10.1149/1945-7111/ac6539.
- [6] S. Baazouzi, N. Feistel, J. Wanner, I. Landwehr, A. Fill, and K. P. Birke, 'Design, Properties, and Manufacturing of Cylindrical Li-Ion Battery Cells—A Generic Overview', *Batteries*, vol. 9, no. 6, Jun. 2023, doi: 10.3390/batteries9060309.
- [7] P. Svens, A. J. Smith, J. Groot, M. J. Lacey, G. Lindbergh, and R. W. Lindstrom, 'Evaluating Performance and Cycle Life Improvements in the Latest Generations of Prismatic Lithium-Ion Batteries', *IEEE Transactions on Transportation Electrification*, vol. 8, no. 3, pp. 3696–3706, Sep. 2022, doi: 10.1109/TTE.2022.3158838.

- [8] M. K. Tran, A. Dacosta, A. Mevawalla, S. Panchal, and M. Fowler, 'Comparative study of equivalent circuit models performance in four common lithium-ion batteries: LFP, NMC, LMO, NCA', *Batteries*, vol. 7, no. 3, Sep. 2021, doi: 10.3390/batteries7030051.
- [9] J. Lu, C. Zhou, Z. Liu, K. S. Lee, and L. Lu, 'LiMn<sub>2</sub>O<sub>4</sub> cathode materials with large porous structure and radial interior channels for lithium ion batteries', *Electrochim Acta*, vol. 212, pp. 553–560, Sep. 2016, doi: 10.1016/j.electacta.2016.07.013.
- [10] P. Yue, 'Introduction of LFP and Ternary Cathode Materials of Lithium Battery', 2023.
- [11] D. Vernardou, 'Recent Report on the Hydrothermal Growth of LiFePO<sub>4</sub> as a Cathode Material', *Coatings*, vol. 12, no. 10, Oct. 2022, doi: 10.3390/coatings12101543.
- [12] C. R. Arro, A. T. I. Mohamed, and N. Bensalah, 'Impact of Ge content on the electrochemical performance of Germanium Oxide/Germanium/ reduced graphene (GeO<sub>2</sub>/Ge/r-GO) hybrid composite anodes for lithium-ion batteries', *Mater Today Commun*, vol. 30, Mar. 2022, doi: 10.1016/j.mtcomm.2022.103151.
- [13] W. Bin Jung *et al.*, 'Three-dimensional SnO<sub>2</sub>nanoparticles synthesized by joule heating as anode materials for lithium ion batteries', *Nano Express*, vol. 3, no. 2, Jun. 2022, doi: 10.1088/2632-959X/ac6e78.
- [14] S. A. D. R. Madhusanka *et al.*, 'TiO<sub>2</sub> microparticles/reduced graphene oxide composite as anode material for lithium ion battery', *Int J Electrochem Sci*, vol. 15, no. 3, pp. 2792–2805, Mar. 2020, doi: 10.20964/2020.03.11.
- [15] J. Choi, W. J. Byun, D. Kang, and J. K. Lee, 'Porous manganese oxide networks as high-capacity and high-rate anodes for lithium-ion batteries', *Energies (Basel)*, vol. 14, no. 5, Mar. 2021, doi: 10.3390/en14051299.

- [16] L. Li, 'Advancements in anode and cathode nanomaterials for high-performance Li-ion batteries', *Applied and Computational Engineering*, vol. 26, no. 1, pp. 193–200, Nov. 2023, doi: 10.54254/2755-2721/26/20230830.
- [17] R. A. Rochman, S. Wahyuningsih, A. H. Ramelan, and Q. A. Hanif, 'Preparation of nitrogen and sulphur Co-doped reduced graphene oxide (rGO-NS) using N and S heteroatom of thiourea', in *IOP Conference Series: Materials Science and Engineering*, Institute of Physics Publishing, May 2019. doi: 10.1088/1757-899X/509/1/012119.
- [18] L. Lu *et al.*, 'One-step: In situ growth of ZnS nanoparticles on reduced graphene oxides and their improved lithium storage performance using sodium carboxymethyl cellulose binder', *RSC Adv*, vol. 8, no. 17, pp. 9125–9133, 2018, doi: 10.1039/c8ra00470f.
- [19] Y. Chen, X. Zhang, Y. Tian, and X. Zhao, 'Synthesis and characterization of silicon nanoparticles inserted into graphene sheets as high performance anode material for lithium ion batteries', *J Nanomater*, vol. 2014, 2014, doi: 10.1155/2014/734751.
- [20] C. Fan *et al.*, 'Hierarchical multi-channels conductive framework constructed with rGO modified natural biochar for high sulfur areal loading self-supporting cathode of lithium-sulfur batteries', *Chemical Engineering Journal Advances*, vol. 9, Mar. 2022, doi: 10.1016/j.ceja.2021.100209.
- [21] E. Venezia, L. Carbone, F. Bonaccorso, and V. Pellegrini, 'Tuning the morphology of sulfur-few layer graphene composites via liquid phase evaporation for battery application', *Nanoscale Adv*, vol. 4, no. 4, pp. 1136–1144, Feb. 2022, doi: 10.1039/d1na00733e.

- [22] T. Tite *et al.*, ‘Pulsed laser deposited V<sub>2</sub>O<sub>3</sub> thin-films on graphene/aluminum foil for micro-battery applications’, *Journal of Electroanalytical Chemistry*, vol. 933, Mar. 2023, doi: 10.1016/j.jelechem.2023.117290.
- [23] X. Guan, K. C. Chan, L. Lei, I. A. Kinloch, and M. A. Bissett, ‘Graphene interleaved SiO<sub>x</sub>/C spheres Via molecular polymerization as high-stability lithium-ion battery anodes’, *Electrochim Acta*, vol. 469, Nov. 2023, doi: 10.1016/j.electacta.2023.143247.
- [24] S. A. Alomari, D. P. Dubal, J. MacLeod, S. Jadhav, C. Padwal, and N. Motta, ‘Nitrogen, phosphorus co-doped holey rGO as a cathode material for Li-ion capacitors (LICs)’, *Appl Surf Sci*, vol. 641, Dec. 2023, doi: 10.1016/j.apsusc.2023.158452.
- [25] H. bing HE, Z. LIU, C. qun PENG, J. LIU, X. feng WANG, and J. ZENG, ‘3D MoS<sub>2</sub>/graphene nanoflowers as anode for advanced lithium-ion batteries’, *Transactions of Nonferrous Metals Society of China (English Edition)*, vol. 32, no. 12, pp. 4041–4049, Dec. 2022, doi: 10.1016/S1003-6326(22)66076-X.
- [26] S. Kalyan, A. Bhosale, P. D. Patil, and N. B. Bahadure, ‘CuS/GO composite for high performance Lithium ion storage’, *Applied Surface Science Advances*, vol. 11, Oct. 2022, doi: 10.1016/j.apsadv.2022.100285.
- [27] G. Zhang, J. You, Q. Chen, Z. Xiong, Y. Wang, and S. Cheng, ‘Mesoporous NiCo<sub>2</sub>S<sub>4</sub>@rGO nanocomposites as sulfur carriers for high performance lithium sulfur batteries’, *Int J Electrochem Sci*, vol. 19, no. 4, Apr. 2024, doi: 10.1016/j.ijoes.2024.100535.
- [28] N. E. Safie, M. A. Azam, C. K. Chiew, M. F. Abdul Aziz, M. N. F. Md Sairi, and A. Takasaki, ‘Structural characterizations and electrochemical performances of rGO-based anode materials for lithium-ion battery’, *Journal of Materials Science:*

